POLITECNICO DI TORINO
Repository ISTITUZIONALE

Optimal sliding friction coefficients for isolated viaducts and bridges: A comparison study

(Article begins on next page)

19 April 2024

OPTIMAL SLIDING FRICTION COEFFICIENTS FOR ISOLATED VIADUCTS AND BRIDGES: A COMPARISON STUDY

P. Castaldo[1], G. Amendola[2]

[1] Department of Structural, Geotechnical and Building Engineering (DISEG), Politecnico di Torino, Turin, Italy (corresponding author). E-mail: paolo.castaldo@polito.it ; pcastaldo@unisa.it

[2] Department of Structural, Geotechnical and Building Engineering (DISEG), Politecnico di Torino, Turin, Italy. E-mail: guglielmo.amendola@polito.it

ABSTRACT

The aim of this work is to evaluate the influence of the pier-abutment-deck interaction on the seismic response of bridges isolated by single concave sliding pendulum isolators (FPS) through a comparison with the results of the seismic response of isolated bridges without considering the presence of the rigid abutment (i.e., isolated viaducts). Two different multi-degree-of-freedom (mdof) models are properly defined to carry out this comparison. In the both mdof models, five vibrational modes are considered to describe the elastic behavior of the reinforced concrete pier and an additional degree of freedom is adopted to analyze the response of the infinitely rigid deck isolated by the seismic devices. The FPS isolator behavior is described through a widespread velocity-dependent model. By means of a non-dimensional formulation of the motion equations with respect to the seismic intensity, a parametric analysis for several structural properties is performed in order to investigate the differences between the two mdof models in relation to the relevant response parameters. The uncertainty in the seismic input is taken into account by means of a set of natural records with different characteristics. Finally, multi-variate non-linear regression relationships are provided to estimate the optimum values of the sliding friction coefficient able to minimize the pier displacements relative to the ground as a function of the structural properties considering or neglecting the presence of the abutment.

KEYWORDS: seismic friction pendulum isolators; bridges; pier-abutment-deck interaction; viaducts; non-dimensional form; optimal friction coefficient.

1 INTRODUCTION

Seismic isolation of bridges allows to uncouple the deck from the horizontal components of the earthquake motion, leading to a substantial reduction of the deck acceleration and, consequently, of the forces transmitted to the pier in comparison to non-isolated bridges as widely demonstrated in many studies dealing with both elastomeric (LRB) and frictional (FPS) isolators [1]-[8]. Jangid [9], assuming a stochastic model of the earthquake ground motion, considered the seismic performance of a bridge equipped with LRB devices, illustrating that there exists an optimal value of the yield strength for which the root mean square absolute acceleration of the deck can be minimized. Closed-form expressions for both the optimum yield strength of the LRBs and corresponding response of the isolated bridge system are proposed. Tongaonkar and Jangid [10] evaluated the effects of soil-structure interaction on the peak responses of a three-span continuous deck bridge isolated by the elastomeric bearings showing their influence to assess the bearing displacements at abutment locations. The results of [11] demonstrate that the isolation can have beneficial effects even for bridges located in medium soil types. A deterministic analysis carried out by [12] examined the influence of coupled vertical and horizontal ground motions on the response of a 3D isolated bridge considering soil-pile-superstructure interaction effects. Considering the soil-structure-interaction effects for seismic-isolated bridges, the study [13] presents a procedure for the selection of optimal intensity measures under the combined strong horizontal and vertical component seismic excitations

with respect to different critical engineering demand parameters. Contextually, friction pendulum system (FPS) devices have been often employed for their capability to provide an isolation period independent of the isolated mass as well as to assure high dissipation and recentering in addition to their longevity and durability properties [14]-[16]. Several experimental and numerical researches have explored the behavior of the FPS isolators [17]-[24]. In [25]-[29], with reference to equivalent multi-degree-of-freedom models, respectively, for base-isolated building frames and isolated bridges with single or double FPS devices, a nondimensionalization of the motion equations for different isolator and system properties has been proposed. The seismic response of isolated multi-span continuous deck bridges is investigated in [31] confirming the effectiveness of simplified models in relation to the flexibility of the deck and of the piers. The seismic response of a bridge isolated with FPS isolators has been analyzed by Kim and Yun [32] highlighting the positive effects of a double concave friction pendulum system on the bridge response. Eröz and DesRoches [33]-[34] studied the effect of modeling parameters and the influence of the design parameters on the response of a three-dimensional multi-span continuous steel girder bridge model seismically isolated by the FPS bearings. Moreover, other works have been more oriented to develop design approaches for the isolators. In this respect, the seismic reliability-based design (SRBD) approach has been proposed and widely discussed in [35]-[37] as a new methodology useful to provide design solutions for seismic devices taking into account the main uncertainties relevant to the problem.

This work aims to evaluate the influence of the pier-abutment-deck interaction on the seismic response of bridges isolated by single concave sliding pendulum isolators (FPS) through a comparison with the results of the seismic response of isolated bridges without considering the presence of the rigid reinforced concrete (RC) abutment (i.e., isolated viaducts). Indeed, two different multi-degree-of-freedom (mdof) models representative, respectively, of a single-column bent viaduct [29] and a multi-span continuous deck bridge [7],[15] are properly defined. Specifically, a six-degree-of-freedom model is used to represent the dynamic behaviour of the both isolated bridge systems. In the both mdof models, five vibrational modes are considered to describe the elastic behavior of the RC pier and an additional degree of freedom is adopted to analyze the response of the infinitely rigid RC deck isolated by the FPS devices. If considered, the presence of the RC abutment is assumed rigid. The FPS isolator behavior is described through a widespread velocity-dependent model. By means of a non-dimensional formulation of the motion equations with respect to the seismic intensity, proposed in [25],[28] and herein extended, a parametric analysis for several structural properties is performed in order to investigate the differences between the two mdof models in relation to the relevant response parameters. The uncertainty in the seismic input is taken into account by means of a set of non-frequent natural records with different characteristics [28]. Finally, multi-variate non-linear regression relationships are provided to estimate the optimum values of the sliding friction coefficient able to minimize the pier displacements relative to the ground as a function of the structural properties and of the seismic input intensity considering or neglecting the rigid presence of the abutment (i.e., single-column bent viaduct and multi-span continuous deck bridge). These non-dimensional expressions can be employed for the preliminary design or retrofit of both single-column bent viaducts and multi-span continuous deck bridges, located in any site, with the purpose to define the optimal friction properties of these seismic devices aimed at assuring an adequate seismic protection.

2 NON-DIMENSIONAL MOTION EQUATIONS FOR BRIDGES ISOLATED BY FPS DEVICES

In the case of a single-column bent viaduct (or neglecting the presence of the abutment) [29], an equivalent 6-degree-of-freedom (dof) model having 5 degrees of freedom for the elastic RC pier and 1 degree of freedom for the rigid RC deck mass equipped with FPS devices is adopted as shown in Fig.1(a). The motion equations, in terms of drifts between the different degrees of freedom, governing the seismic response when the isolated system is subjected to the seismic input along the longitudinal direction, $\ddot{u}_g(t)$, are:

$$
\begin{bmatrix}
m_d & m_d & m_d & m_d & m_d & m_d \\
0 & m_{p5} & m_{p5} & m_{p5} & m_{p5} & m_{p5} \\
0 & 0 & m_{p4} & m_{p4} & m_{p4} & m_{p4} \\
0 & 0 & 0 & m_{p3} & m_{p3} & m_{p3} \\
0 & 0 & 0 & 0 & m_{p2} & m_{p2} \\
0 & 0 & 0 & 0 & 0 & m_{p1}
\end{bmatrix}
\begin{bmatrix}
\ddot{u}_d(t) \\
\ddot{u}_{p5}(t) \\
\ddot{u}_{p4}(t) \\
\ddot{u}_{p3}(t) \\
\ddot{u}_{p2}(t) \\
\ddot{u}_{p1}(t)
\end{bmatrix}
+
\begin{bmatrix}
c_d & 0 & 0 & 0 & 0 & 0 \\
-c_d & c_{p5} & 0 & 0 & 0 & 0 \\
0 & -c_{p5} & c_{p4} & 0 & 0 & 0 \\
0 & 0 & -c_{p4} & c_{p3} & 0 & 0 \\
0 & 0 & 0 & -c_{p3} & c_{p2} & 0 \\
0 & 0 & 0 & 0 & -c_{p2} & c_{p1}
\end{bmatrix}
\begin{bmatrix}
\dot{u}_d(t) \\
\dot{u}_{p5}(t) \\
\dot{u}_{p4}(t) \\
\dot{u}_{p3}(t) \\
\dot{u}_{p2}(t) \\
\dot{u}_{p1}(t)
\end{bmatrix}
+
$$

$$
+
\begin{bmatrix}
m_d g/R & 0 & 0 & 0 & 0 & 0 \\
-m_d g/R & k_{p5} & 0 & 0 & 0 & 0 \\
0 & -k_{p5} & k_{p4} & 0 & 0 & 0 \\
0 & 0 & -k_{p4} & k_{p3} & 0 & 0 \\
0 & 0 & 0 & -k_{p3} & k_{p2} & 0 \\
0 & 0 & 0 & 0 & -k_{p2} & k_{p1}
\end{bmatrix}
\begin{bmatrix}
u_d(t) \\
u_{p5}(t) \\
u_{p4}(t) \\
u_{p3}(t) \\
u_{p2}(t) \\
u_{p1}(t)
\end{bmatrix}
+
\begin{bmatrix}
m_d g\,\mu(\dot{u}_d(t))\,\mathrm{sgn}(\dot{u}_d(t)) \\
-m_d g\,\mu(\dot{u}_d(t))\,\mathrm{sgn}(\dot{u}_d(t)) \\
0 \\
0 \\
0 \\
0
\end{bmatrix}
= +\ddot{u}_g(t) \cdot
\begin{bmatrix}
-m_d \\
-m_{p5} \\
-m_{p4} \\
-m_{p3} \\
-m_{p2} \\
-m_{p1}
\end{bmatrix}
\tag{1}
$$

where u_d denotes the horizontal displacement of the deck relative to pier, $u_{p1}, u_{p2}, u_{p3}, u_{p4}, u_{p5}$ are the pier displacements relative between two consecutive dof, $m_d, m_{p1}, m_{p2}, m_{p3}, m_{p4}, m_{p5}$ respectively the mass of the deck and of each dof of the pier, $k_{p1}, k_{p2}, k_{p3}, k_{p4}, k_{p5}$ and $c_{p1}, c_{p2}, c_{p3}, c_{p4}, c_{p5}$ respectively the stiffness and inherent viscous damping coefficient of each dof of the pier, c_d the bearing viscous damping factor, t the time instant, the dot differentiation over time, and the FPS bearing force $F_{FPS}(t)$ [38]-[39] (Fig.1(g)-(h)) applies as follows:

$$
F_{FPS}(t) = k_d u_d(t) + \mu(\dot{u}_d) m_d g\,\mathrm{sgn}(\dot{u}_d)
\tag{1}
$$

where $k_d = W/R = m_d g/R$, g is the gravity constant, R is the radius of curvature of the FPS device, $\mu(\dot{u}_d(t))$ the sliding friction coefficient, which depends on the bearing slip horizontal velocity $\dot{u}_d(t)$ [37], and $sgn(\cdot)$ denotes the sign function. Eq.(2) is based on the hypothesis of neglecting the vertical displacement component as well as for high values of R [37]. As reported in [16], the fundamental vibration period of an isolated bridge, $T_d = 2\pi\sqrt{R/g}$, corresponding to the pendulum behaviour component, depends only on the radius of curvature R.

According to [18]-[21], the sliding friction coefficient of teflon-steel interfaces can be expressed by the following equation:

$$
\mu(\dot{u}_d) = \mu_{\max} - (\mu_{\max} - \mu_{\min}) \cdot \exp(-\alpha|\dot{u}_d|)
\tag{3}
$$

where $\mu_{\max}$ and $\mu_{\min}$ represent, respectively, the maximum value of sliding friction coefficient attained at large velocities and the value at zero velocity. In this study, it is considered that $\mu_{\max} = 3\mu_{\min}$ with the exponent α equal to 30 [25].

As also discussed in [37], considering the maximum value of the sliding friction coefficient, the effective stiffness of the FPS bearings $k_{eff} = W(1/ + \mu_{\max}/u_d)$ (Fig.1(h)) as well as the corresponding effective isolated period $T_{d,eff}$ [40],[41] (Fig. 1(h)) can be computed depending on the displacement demand.

Note that Eq.(1) is representative of the dynamic behaviour of a single-column bent viaduct as long as the bridge is straight and consists of a large number of equal spans and piers of equal height or stiffness and with a superstructure (deck) that can be assumed to move as a rigid body [42].

By simply dividing Eq. (1) with respect to the deck mass m_d, the following equations apply:

$$
\begin{bmatrix}
1 & 1 & 1 & 1 & 1 & 1 \\
0 & \lambda_{p5} & \lambda_{p5} & \lambda_{p5} & \lambda_{p5} & \lambda_{p5} \\
0 & 0 & \lambda_{p4} & \lambda_{p4} & \lambda_{p4} & \lambda_{p4} \\
0 & 0 & 0 & \lambda_{p3} & \lambda_{p3} & \lambda_{p3} \\
0 & 0 & 0 & 0 & \lambda_{p2} & \lambda_{p2} \\
0 & 0 & 0 & 0 & 0 & \lambda_{p1}
\end{bmatrix}
\cdot
\begin{bmatrix}
\ddot{u}_d(t) \\
\ddot{u}_{p5}(t) \\
\ddot{u}_{p4}(t) \\
\ddot{u}_{p3}(t) \\
\ddot{u}_{p2}(t) \\
\ddot{u}_{p1}(t)
\end{bmatrix}
+
$$

$$
+
\begin{bmatrix}
2\xi_d\omega_d & 0 & 0 & 0 & 0 & 0 \\
-2\xi_d\omega_d & 2\xi_{p5}\omega_{p5}\lambda_{p5} & 0 & 0 & 0 & 0 \\
0 & -2\xi_{p5}\omega_{p5}\lambda_{p5} & 2\xi_{p4}\omega_{p4}\lambda_{p4} & 0 & 0 & 0 \\
0 & 0 & -2\xi_{p4}\omega_{p4}\lambda_{p4} & 2\xi_{p3}\omega_{p3}\lambda_{p3} & 0 & 0 \\
0 & 0 & 0 & -2\xi_{p3}\omega_{p3}\lambda_{p3} & 2\xi_{p2}\omega_{p2}\lambda_{p2} & 0 \\
0 & 0 & 0 & 0 & -2\xi_{p2}\omega_{p2}\lambda_{p2} & 2\xi_{p1}\omega_{p1}\lambda_{p1}
\end{bmatrix}
\cdot
\begin{bmatrix}
\dot{u}_d(t) \\
\dot{u}_{p5}(t) \\
\dot{u}_{p4}(t) \\
\dot{u}_{p3}(t) \\
\dot{u}_{p2}(t) \\
\dot{u}_{p1}(t)
\end{bmatrix}
+
$$

$$
+
\begin{bmatrix}
g/R & 0 & 0 & 0 & 0 & 0 \\
-g/R & \lambda_{p5}\omega_{p5}^2 & 0 & 0 & 0 & 0 \\
0 & -\lambda_{p5}\omega_{p5}^2 & \lambda_{p4}\omega_{p4}^2 & 0 & 0 & 0 \\
0 & 0 & -\lambda_{p4}\omega_{p4}^2 & \lambda_{p3}\omega_{p3}^2 & 0 & 0 \\
0 & 0 & 0 & -\lambda_{p3}\omega_{p3}^2 & \lambda_{p2}\omega_{p2}^2 & 0 \\
0 & 0 & 0 & 0 & -\lambda_{p2}\omega_{p2}^2 & \lambda_{p1}\omega_{p1}^2
\end{bmatrix}
\cdot
\begin{bmatrix}
u_d(t) \\
u_{p5}(t) \\
u_{p4}(t) \\
u_{p3}(t) \\
u_{p2}(t) \\
u_{p1}(t)
\end{bmatrix}
+
\begin{bmatrix}
g\mu(\dot{u}_d(t))\,\mathrm{sgn}(\dot{u}_d(t)) \\
-g\mu(\dot{u}_d(t))\,\mathrm{sgn}(\dot{u}_d(t)) \\
0 \\
0 \\
0 \\
0
\end{bmatrix}
= +\ddot{u}_g(t)\cdot
\begin{bmatrix}
-1 \\
-\lambda_{p5} \\
-\lambda_{p4} \\
-\lambda_{p3} \\
-\lambda_{p2} \\
-\lambda_{p1}
\end{bmatrix}
\tag{4}
$$

and the following ratios are introduced:

$$
\omega_d = \sqrt{\frac{k_d}{m_d}}, \quad \omega_{pi} = \sqrt{\frac{k_{pi}}{m_{pi}}}, \quad \xi_d = \frac{c_d}{2m_d\omega_d}, \quad \xi_{pi} = \frac{c_{pi}}{2m_{pi}\omega_{pi}}, \quad \lambda_{pi} = \frac{m_{pi}}{m_d} \quad with\ i = 1,...,5
\tag{5}
$$

The first two terms denote, respectively, the circular frequency of vibration of the isolated deck and of the i-th lumped mass of the pier; ξ_d is the damping factor of the isolated deck, ξ_{pi} is the damping factor corresponding to the i-th dof in which the pier has been discretized. The last term represents the i-th mass ratio between the i-th lumped mass of the pier and the deck mass.

With the aim to extend the non-dimensionalization with respect to the seismic intensity proposed by [25]-[26],[28], let us introduce the time scale $\tau = t\omega_d$, in which $\omega_d = \sqrt{k_d/m_d}$ is the fundamental circular frequency of the isolated system with infinitely rigid superstructure, and the seismic intensity scale a_0, so that $\ddot{u}_g(t) = a_0\ell(\tau)$, where $\ell(\tau)$ is a non-dimensional function of time describing the seismic input time-history, the following non-dimensional equations (i.e., normalised with respect to the seismic intensity) can be obtained:

$$\begin{bmatrix} 1 & 1 & 1 & 1 & 1 & 1 \\ 0 & \lambda_{p5} & \lambda_{p5} & \lambda_{p5} & \lambda_{p5} & \lambda_{p5} \\ 0 & 0 & \lambda_{p4} & \lambda_{p4} & \lambda_{p4} & \lambda_{p4} \\ 0 & 0 & 0 & \lambda_{p3} & \lambda_{p3} & \lambda_{p3} \\ 0 & 0 & 0 & 0 & \lambda_{p2} & \lambda_{p2} \\ 0 & 0 & 0 & 0 & 0 & \lambda_{p1} \end{bmatrix} \begin{bmatrix} \ddot{\psi}_d(\tau) \\ \ddot{\psi}_{p5}(\tau) \\ \ddot{\psi}_{p4}(\tau) \\ \ddot{\psi}_{p3}(\tau) \\ \ddot{\psi}_{p2}(\tau) \\ \ddot{\psi}_{p1}(\tau) \end{bmatrix} +$$

$$+ \begin{bmatrix} 2\xi_d & 0 & 0 & 0 & 0 & 0 \\ -2\xi_d & 2\xi_{p5}\dfrac{\omega_{p5}}{\omega_d}\lambda_{p5} & 0 & 0 & 0 & 0 \\ 0 & -2\xi_{p5}\dfrac{\omega_{p5}}{\omega_d}\lambda_{p5} & 2\xi_{p4}\dfrac{\omega_{p4}}{\omega_d}\lambda_{p4} & 0 & 0 & 0 \\ 0 & 0 & -2\xi_{p4}\dfrac{\omega_{p4}}{\omega_d}\lambda_{p4} & 2\xi_{p3}\dfrac{\omega_{p3}}{\omega_d}\lambda_{p3} & 0 & 0 \\ 0 & 0 & 0 & -2\xi_{p3}\dfrac{\omega_{p3}}{\omega_d}\lambda_{p3} & 2\xi_{p2}\dfrac{\omega_{p2}}{\omega_d}\lambda_{p2} & 0 \\ 0 & 0 & 0 & 0 & -2\xi_{p2}\dfrac{\omega_{p2}}{\omega_d}\lambda_{p2} & 2\xi_{p1}\dfrac{\omega_{p1}}{\omega_d}\lambda_{p1} \end{bmatrix} \cdot \begin{bmatrix} \dot{\psi}_d(\tau) \\ \dot{\psi}_{p5}(\tau) \\ \dot{\psi}_{p4}(\tau) \\ \dot{\psi}_{p3}(\tau) \\ \dot{\psi}_{p2}(\tau) \\ \dot{\psi}_{p1}(\tau) \end{bmatrix} +$$

$$+ \begin{bmatrix} 1 & 0 & 0 & 0 & 0 & 0 \\ -1 & \lambda_{p5}\dfrac{\omega_{p5}^2}{\omega_d^2} & 0 & 0 & 0 & 0 \\ 0 & -\lambda_{p5}\dfrac{\omega_{p5}^2}{\omega_d^2} & \lambda_{p4}\dfrac{\omega_{p4}^2}{\omega_d^2} & 0 & 0 & 0 \\ 0 & 0 & -\lambda_{p4}\dfrac{\omega_{p4}^2}{\omega_d^2} & \lambda_{p3}\dfrac{\omega_{p3}^2}{\omega_d^2} & 0 & 0 \\ 0 & 0 & 0 & -\lambda_{p3}\dfrac{\omega_{p3}^2}{\omega_d^2} & \lambda_{p2}\dfrac{\omega_{p2}^2}{\omega_d^2} & 0 \\ 0 & 0 & 0 & 0 & -\lambda_{p2}\dfrac{\omega_{p2}^2}{\omega_d^2} & \lambda_{p1}\dfrac{\omega_{p1}^2}{\omega_d^2} \end{bmatrix} \cdot \begin{bmatrix} \psi_d(\tau) \\ \psi_{p5}(\tau) \\ \psi_{p4}(\tau) \\ \psi_{p3}(\tau) \\ \psi_{p2}(\tau) \\ \psi_{p1}(\tau) \end{bmatrix} + \begin{bmatrix} \dfrac{g\mu(\dot{\psi}_d(\tau))}{a_0}\mathrm{sgn}(\dot{\psi}_d(\tau)) \\ -\dfrac{g\mu(\dot{\psi}_d(\tau))}{a_0}\mathrm{sgn}(\dot{\psi}_d(\tau)) \\ 0 \\ 0 \\ 0 \\ 0 \end{bmatrix} = +l(\tau)\cdot \begin{bmatrix} -1 \\ -\lambda_{p5} \\ -\lambda_{p4} \\ -\lambda_{p3} \\ -\lambda_{p2} \\ -\lambda_{p1} \end{bmatrix}$$

$$(6)$$

The following non-dimensional parameters $\psi_{u_d} = \dfrac{u_{d,peak}\,\omega_d^2}{a_0}$ and $\psi_{u_p} = \dfrac{u_{p,peak}\,\omega_d^2}{a_0} = \dfrac{\left(\sum\limits_{i=1}^{5} u_{p_i}\right)_{peak}\omega_d^2}{a_0}$

describe the peak dynamic response of the deck and of pier, respectively. Moreover, from Eq.(6), it is possible to observe that the five non-dimensional Π terms [25]-[26],[28],[43]-[44] that control the system non-dimensional response are:

$$\Pi_{\omega i} = \frac{\omega_{pi}}{\omega_d}, \quad \Pi_{\lambda pi} = \lambda_{pi} = \frac{m_{pi}}{m_d}, \quad \Pi_\mu(\dot{\psi}_d) = \frac{\mu(\dot{\psi}_d)g}{a_0}, \quad \Pi_{\xi_d} = \xi_d, \quad \Pi_{\xi_{pi}} = \xi_{pi} \quad \text{with } i = 1,...,5 \quad (7a,b,c,d,e)$$

in particular, $\Pi_{\omega i}$ represents the i-th frequency ratio, $\Pi_{\lambda pi}$ is the i-th mass ratio as previously defined, $\Pi_{\xi_{pi}}$ and Π_{ξ_d} are the inherent viscous damping related to the i-th dof of the pier and to the isolator/deck, respectively. Regarding the control parameters of the pier, indeed, the parameters ω_{pi} are related to the fundamental vibration pulsation ω_p (the first vibration mode) as well as the sum of the mass ratios is related to the overall mass ratio $\Pi_\lambda = \lambda_p = \sum\limits_{i=1}^{5} m_{pi}/m_d$ and, finally, all the damping

factors are assumed equal to $\Pi_{\xi_p} = \xi_p$. The term Π_μ denotes the isolator strength, which depends on both the friction coefficient $\mu(\dot{\psi}_d)$ and the seismic intensity. Since the sliding friction coefficient is a velocity-dependent parameter, Π_μ is considered in its stead as follows [25]:
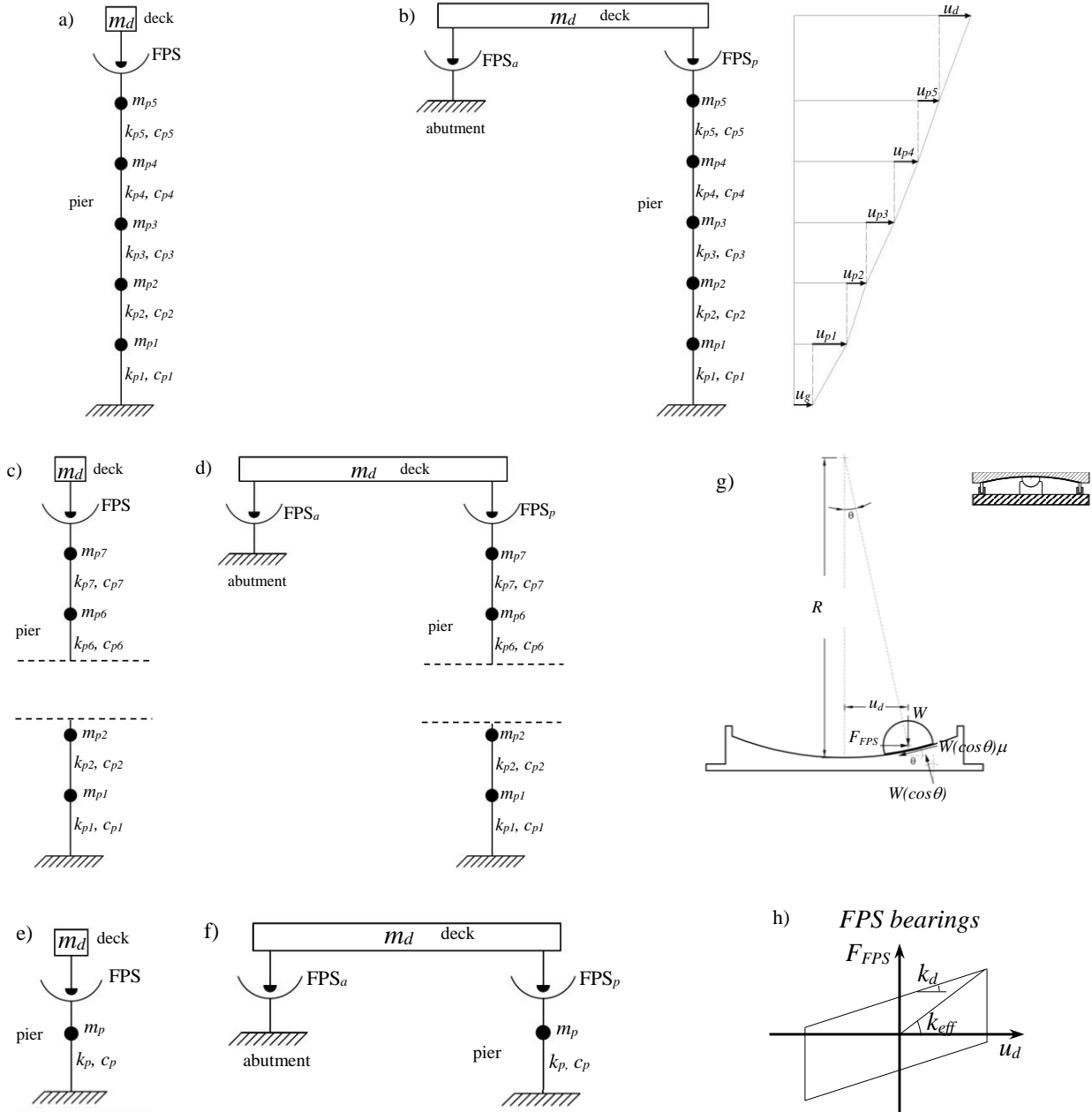
$$\Pi_\mu^* = \frac{\mu_{max} g}{a_0} \tag{8}$$

Fig. 1. 6dof model of a bridge isolated by FPS bearings without pier-abutment-deck interaction (i.e., viaduct) (a); 6dof model of a bridge isolated by FPS bearings considering pier-abutment-deck interaction (b); 8dof models (c)-(d); 2dof models (e)-(f); FPS parameters (g) and response (h).

Referring to a multi-span continuous deck bridge (e.g., three-span continuous deck bridge) [7],[15], the presence of the rigid RC abutment is considered (Fig. 1(b)), so, the dimensional equations that govern the motion of this new system change because of the term related to the isolator on the abutment, as follows:

$$
\begin{bmatrix}
m_d & m_d & m_d & m_d & m_d & m_d \\
0 & m_{p5} & m_{p5} & m_{p5} & m_{p5} & m_{p5} \\
0 & 0 & m_{p4} & m_{p4} & m_{p4} & m_{p4} \\
0 & 0 & 0 & m_{p3} & m_{p3} & m_{p3} \\
0 & 0 & 0 & 0 & m_{p2} & m_{p2} \\
0 & 0 & 0 & 0 & 0 & m_{p1}
\end{bmatrix}
\cdot
\begin{bmatrix}
\ddot{u}_d(t) \\
\ddot{u}_{p5}(t) \\
\ddot{u}_{p4}(t) \\
\ddot{u}_{p3}(t) \\
\ddot{u}_{p2}(t) \\
\ddot{u}_{p1}(t)
\end{bmatrix}
+
\begin{bmatrix}
c_d & 0 & 0 & 0 & 0 & 0 \\
-c_d & c_{p5} & 0 & 0 & 0 & 0 \\
0 & -c_{p5} & c_{p4} & 0 & 0 & 0 \\
0 & 0 & -c_{p4} & c_{p3} & 0 & 0 \\
0 & 0 & 0 & -c_{p3} & c_{p2} & 0 \\
0 & 0 & 0 & 0 & -c_{p2} & c_{p1}
\end{bmatrix}
\cdot
\begin{bmatrix}
\dot{u}_d(t) \\
\dot{u}_{p5}(t) \\
\dot{u}_{p4}(t) \\
\dot{u}_{p3}(t) \\
\dot{u}_{p2}(t) \\
\dot{u}_{p1}(t)
\end{bmatrix}
+
$$

$$
+
\begin{bmatrix}
\dfrac{m_d}{2}g/R_p+\dfrac{m_d}{2}g/R_a & \dfrac{m_d}{2}g/R_a & \dfrac{m_d}{2}g/R_a & \dfrac{m_d}{2}g/R_a & \dfrac{m_d}{2}g/R_a & \dfrac{m_d}{2}g/R_a \\
-\dfrac{m_d}{2}g/R_p & k_{p5} & 0 & 0 & 0 & 0 \\
0 & -k_{p5} & k_{p4} & 0 & 0 & 0 \\
0 & 0 & -k_{p4} & k_{p3} & 0 & 0 \\
0 & 0 & 0 & -k_{p3} & k_{p2} & 0 \\
0 & 0 & 0 & 0 & -k_{p2} & k_{p1}
\end{bmatrix}
\cdot
\begin{bmatrix}
u_d \\
u_{p5} \\
u_{p4} \\
u_{p3} \\
u_{p2} \\
u_{p1}
\end{bmatrix}
+
$$

$$
+
\begin{bmatrix}
\dfrac{m_d}{2}g\mu_p(\dot{u}_d(t))\,\mathrm{sgn}(\dot{u}_d(t))+\dfrac{m_d}{2}g\mu_a\!\left(\dot{u}_d(t)+\sum_{i=1}^{5}\dot{u}_{pi}(t)\right)\mathrm{sgn}\!\left(\dot{u}_d(t)+\sum_{i=1}^{5}\dot{u}_{pi}(t)\right) \\
-\dfrac{m_d}{2}g\mu_p(\dot{u}_d(t))\,\mathrm{sgn}(\dot{u}_d(t)) \\
0 \\
0 \\
0 \\
0
\end{bmatrix}
= +\ddot{u}_g(t)\cdot
\begin{bmatrix}
-m_d \\
-m_{p5} \\
-m_{p4} \\
-m_{p3} \\
-m_{p2} \\
-m_{p1}
\end{bmatrix}
\tag{9}
$$

where the FPS properties are recognized by the subscript "*a*" and "*p*" with reference to abutment and pier, respectively, and their forces apply:

$$
F_p(t)=\frac{m_d g}{2}\left[\frac{1}{R_p}u_d(t)+\mu_p(\dot{u}_d)\,\mathrm{sgn}(\dot{u}_d)\right]
$$

$$
F_a(t)=\frac{m_d g}{2}\left[\frac{1}{R_a}\left(u_d(t)+\sum_{i=1}^{5}u_{pi}(t)\right)+\mu_a\left(\dot{u}_d(t)+\sum_{i=1}^{5}\dot{u}_{pi}(t)\right)\mathrm{sgn}\left(\dot{u}_d(t)+\sum_{i=1}^{5}\dot{u}_{pi}(t)\right)\right]
\tag{10a,b}
$$

where $F_a(t)$ is the reaction force associated to the isolator placed over the abutment and $F_p(t)$ is the same of Eq.s (1)-(2), with the only difference that the deck mass supported by the isolator on the pier is the half of the total one. Furthermore, note that, differently to the reaction force of the seismic device on the pier, the reaction force as well as the friction coefficient related to the abutment isolator depend on both the horizontal velocity and displacement [37] of the deck with respect to the ground. By dividing Eq. (7) by the mass deck m_d, the following equation system is obtained:

$$
\begin{bmatrix}
1 & 1 & 1 & 1 & 1 & 1 \\
0 & \lambda_{p5} & \lambda_{p5} & \lambda_{p5} & \lambda_{p5} & \lambda_{p5} \\
0 & 0 & \lambda_{p4} & \lambda_{p4} & \lambda_{p4} & \lambda_{p4} \\
0 & 0 & 0 & \lambda_{p3} & \lambda_{p3} & \lambda_{p3} \\
0 & 0 & 0 & 0 & \lambda_{p2} & \lambda_{p2} \\
0 & 0 & 0 & 0 & 0 & \lambda_{p1}
\end{bmatrix}
\cdot
\begin{bmatrix}
\ddot{u}_d(t) \\
\ddot{u}_{p5}(t) \\
\ddot{u}_{p4}(t) \\
\ddot{u}_{p3}(t) \\
\ddot{u}_{p2}(t) \\
\ddot{u}_{p1}(t)
\end{bmatrix} +
$$

$$
+
\begin{bmatrix}
2\xi_d\omega_d & 0 & 0 & 0 & 0 & 0 \\
-2\xi_d\omega_d & 2\xi_{p5}\omega_{p5}\lambda_{p5} & 0 & 0 & 0 & 0 \\
0 & -2\xi_{p5}\omega_{p5}\lambda_{p5} & 2\xi_{p4}\omega_{p4}\lambda_{p4} & 0 & 0 & 0 \\
0 & 0 & -2\xi_{p4}\omega_{p4}\lambda_{p4} & 2\xi_{p3}\omega_{p3}\lambda_{p3} & 0 & 0 \\
0 & 0 & 0 & -2\xi_{p3}\omega_{p3}\lambda_{p3} & 2\xi_{p2}\omega_{p2}\lambda_{p2} & 0 \\
0 & 0 & 0 & 0 & -2\xi_{p2}\omega_{p2}\lambda_{p2} & 2\xi_{p1}\omega_{p1}\lambda_{p1}
\end{bmatrix}
\cdot
\begin{bmatrix}
\dot{u}_d(t) \\
\dot{u}_{p5}(t) \\
\dot{u}_{p4}(t) \\
\dot{u}_{p3}(t) \\
\dot{u}_{p2}(t) \\
\dot{u}_{p1}(t)
\end{bmatrix} +
$$

$$
+
\begin{bmatrix}
\frac{g}{2}/R_p+\frac{g}{2}/R_a & \frac{g}{2}/R_a & \frac{g}{2}/R_a & \frac{g}{2}/R_a & \frac{g}{2}/R_a & \frac{g}{2}/R_a \\
-\frac{g}{2}/R_p & \lambda_{p5}\omega_{p5}^2 & 0 & 0 & 0 & 0 \\
0 & -\lambda_{p5}\omega_{p5}^2 & \lambda_{p4}\omega_{p4}^2 & 0 & 0 & 0 \\
0 & 0 & -\lambda_{p4}\omega_{p4}^2 & \lambda_{p3}\omega_{p3}^2 & 0 & 0 \\
0 & 0 & 0 & -\lambda_{p3}\omega_{p3}^2 & \lambda_{p2}\omega_{p2}^2 & 0 \\
0 & 0 & 0 & 0 & -\lambda_{p2}\omega_{p2}^2 & \lambda_{p1}\omega_{p1}^2
\end{bmatrix}
\cdot
\begin{bmatrix}
u_d(t) \\
u_{p5}(t) \\
u_{p4}(t) \\
u_{p3}(t) \\
u_{p2}(t) \\
u_{p1}(t)
\end{bmatrix} +
$$

$$
+
\begin{bmatrix}
\frac{g}{2}\mu_p(\dot{u}_d(t))\mathrm{sgn}(\dot{u}_d(t))+\frac{g}{2}\mu_a(\dot{u}_d(t)+\sum_{i=1}^{5}\dot{u}_{pi}(t))\cdot\mathrm{sgn}(\dot{u}_d(t)+\sum_{i=1}^{5}\dot{u}_{pi}(t)) \\
-\frac{g}{2}\mu_p(\dot{u}_d(t))\mathrm{sgn}(\dot{u}_d(t)) \\
0 \\
0 \\
0 \\
0
\end{bmatrix}
= +\ddot{u}_g(t)\cdot
\begin{bmatrix}
-1 \\
-\lambda_{p5} \\
-\lambda_{p4} \\
-\lambda_{p3} \\
-\lambda_{p2} \\
-\lambda_{p1}
\end{bmatrix}
\tag{11}
$$

in which the terms are the same expressed in Eq. (4).

Similarly to Eq. (6), and assuming that the radii of curvature R_a and R_p are equal, the non-dimensional equations taking into account the presence of the rigid abutment can be derived as follows:

$$
\begin{bmatrix}
1 & 1 & 1 & 1 & 1 & 1 \\
0 & \lambda_{p5} & \lambda_{p5} & \lambda_{p5} & \lambda_{p5} & \lambda_{p5} \\
0 & 0 & \lambda_{p4} & \lambda_{p4} & \lambda_{p4} & \lambda_{p4} \\
0 & 0 & 0 & \lambda_{p3} & \lambda_{p3} & \lambda_{p3} \\
0 & 0 & 0 & 0 & \lambda_{p2} & \lambda_{p2} \\
0 & 0 & 0 & 0 & 0 & \lambda_{p1}
\end{bmatrix}
\cdot
\begin{bmatrix}
\ddot{\psi}_d(\tau) \\
\ddot{\psi}_{p5}(\tau) \\
\ddot{\psi}_{p4}(\tau) \\
\ddot{\psi}_{p3}(\tau) \\
\ddot{\psi}_{p2}(\tau) \\
\ddot{\psi}_{p1}(\tau)
\end{bmatrix}
+
$$

$$
+
\begin{bmatrix}
2\xi_d & 0 & 0 & 0 & 0 & 0 \\
-2\xi_d & 2\xi_{p5}\dfrac{\omega_{p5}}{\omega_d}\lambda_{p5} & 0 & 0 & 0 & 0 \\
0 & -2\xi_{p5}\dfrac{\omega_{p5}}{\omega_d}\lambda_{p5} & 2\xi_{p4}\dfrac{\omega_{p4}}{\omega_d}\lambda_{p4} & 0 & 0 & 0 \\
0 & 0 & -2\xi_{p4}\dfrac{\omega_{p4}}{\omega_d}\lambda_{p4} & 2\xi_{p3}\dfrac{\omega_{p3}}{\omega_d}\lambda_{p3} & 0 & 0 \\
0 & 0 & 0 & -2\xi_{p3}\dfrac{\omega_{p3}}{\omega_d}\lambda_{p3} & 2\xi_{p2}\dfrac{\omega_{p2}}{\omega_d}\lambda_{p2} & 0 \\
0 & 0 & 0 & 0 & -2\xi_{p2}\dfrac{\omega_{p2}}{\omega_d}\lambda_{p2} & 2\xi_{p1}\dfrac{\omega_{p1}}{\omega_d}\lambda_{p1}
\end{bmatrix}
\cdot
\begin{bmatrix}
\dot{\psi}_d(\tau) \\
\dot{\psi}_{p5}(\tau) \\
\dot{\psi}_{p4}(\tau) \\
\dot{\psi}_{p3}(\tau) \\
\dot{\psi}_{p2}(\tau) \\
\dot{\psi}_{p1}(\tau)
\end{bmatrix}
+
$$

$$
+
\begin{bmatrix}
1 & \dfrac{1}{2} & \dfrac{1}{2} & \dfrac{1}{2} & \dfrac{1}{2} & \dfrac{1}{2} \\
-\dfrac{1}{2} & \lambda_{p5}\dfrac{\omega_{p5}^2}{\omega_d^2} & 0 & 0 & 0 & 0 \\
0 & -\lambda_{p5}\dfrac{\omega_{p5}^2}{\omega_d^2} & \lambda_{p4}\dfrac{\omega_{p4}^2}{\omega_d^2} & 0 & 0 & 0 \\
0 & 0 & -\lambda_{p4}\dfrac{\omega_{p4}^2}{\omega_d^2} & \lambda_{p3}\dfrac{\omega_{p3}^2}{\omega_d^2} & 0 & 0 \\
0 & 0 & 0 & -\lambda_{p3}\dfrac{\omega_{p3}^2}{\omega_d^2} & \lambda_{p2}\dfrac{\omega_{p2}^2}{\omega_d^2} & 0 \\
0 & 0 & 0 & 0 & -\lambda_{p2}\dfrac{\omega_{p2}^2}{\omega_d^2} & \lambda_{p1}\dfrac{\omega_{p1}^2}{\omega_d^2}
\end{bmatrix}
\cdot
\begin{bmatrix}
\psi_d(\tau) \\
\psi_{p5}(\tau) \\
\psi_{p4}(\tau) \\
\psi_{p3}(\tau) \\
\psi_{p2}(\tau) \\
\psi_{p1}(\tau)
\end{bmatrix}
+
$$

$$
+
\begin{bmatrix}
\dfrac{g\,\mu_p(\dot{\psi}_d(\tau))}{2a_0}\mathrm{sgn}(\dot{\psi}_d(\tau)) + \dfrac{g}{2}\mu_a\!\left(\dot{\psi}_d(\tau)+\displaystyle\sum_{i=1}^{5}\dot{\psi}_{pi}(\tau)\right)\cdot\mathrm{sgn}\!\left(\dot{\psi}_d(\tau)+\displaystyle\sum_{i=1}^{5}\dot{\psi}_{pi}(\tau)\right) \\
-\dfrac{g\,\mu_p(\dot{\psi}_d)}{2a_0}\mathrm{sgn}(\dot{\psi}_d(\tau)) \\
0 \\
0 \\
0 \\
0
\end{bmatrix}
= +l(\tau)\cdot
\begin{bmatrix}
-1 \\
-\lambda_{p5} \\
-\lambda_{p4} \\
-\lambda_{p3} \\
-\lambda_{p2} \\
-\lambda_{p1}
\end{bmatrix}
\tag{12}
$$

Note that, the non-dimensional parameters, that derive from Eq.(12), are the same of Eq.s (6)-(7) with a distinction as follows. The normalized friction coefficients for the FPS devices on the pier and on the abutment apply, respectively:

$$
\Pi_{\mu p}\left(\dot{\psi}_d\right) = \frac{\mu_p\left(\dot{\psi}_d\right)g}{a_0}, \quad
\Pi_{\mu a}\left(\dot{\psi}_d + \sum_{i=1}^{5}\dot{\psi}_{pi}\right) = \frac{\mu_a\left(\dot{\psi}_d + \displaystyle\sum_{i=1}^{5}\dot{\psi}_{pi}\right)g}{a_0}
\tag{13a,b}
$$

and since these parameters depend on the response through the corresponding velocities, each one is used in its stead as follows:

$$\Pi_{\mu p}{}^* = \frac{\mu_{p,\max} g}{a_0} \ , \quad \Pi_{\mu a}{}^* = \frac{\mu_{a,\max} g}{a_0} \tag{14}$$

It is worth underlining that even if the two FPS devices are equal, $\Pi_{\mu p}{}^* = \Pi_{\mu a}{}^*$, during the dynamic response the terms of Eq.(13) depend on different velocities.

Note that, for the both configurations, the stiffness contribution of non-structural elements, such as kerbs, parapet walls and wearing coat, is neglected. Similarly, the soil-structure interaction as well as the vertical component and bi-directional or asynchronous effects of the earthquake ground motions are neglected [7],[15]. All these effects are worthy to be investigated in future developments adopting specific assumptions as widely commented in [12],[13].

3   RECORD-TO-RECORD VARIABILITY AND INTENSITY MEASURE

3.1   Seismic records

In this analysis, the record-to-record variability is considered using 30 non-frequent [28],[45]-[46] seismic records selected from 19 seismic different events [47]-[49]. Table 1 reports the details of the earthquakes used for the study.

Table 1. Seismic records used and them characteristics.

#	Year	Earthquake Name	Recording Station Name	Vs$_{30}$ [m/sec]	Source (Fault Type)	M [-]	R [km]	PGA$_{max}$ [g]
1	1994	Northridge	Beverly Hills - Mulhol	356	Thrust	6.7	13.3	0.52
2	1994	Northridge	Canyon Country-WLC	309	Thrust	6.7	26.5	0.48
3	1994	Northridge	LA – Hollywood Stor	316	Thrust	6.7	22.9	0.36
4	1999	Duzce, Turkey	Bolu	326	Strike-slip	7.1	41.3	0.82
5	1999	Hector Mine	Hector	685	Strike-slip	7.1	26.5	0.34
6	1979	Imperial Valley	Delta	275	Strike-slip	6.5	33.7	0.35
7	1979	Imperial Valley	El Centro Array #11	196	Strike-slip	6.5	29.4	0.38
8	1995	Kobe, Japan	Nishi-Akashi	609	Strike-slip	6.9	8.7	0.51
9	1995	Kobe, Japan	Shin-Osaka	256	Strike-slip	6.9	46	0.24
10	1999	Kocaeli, Turkey	Duzce	276	Strike-slip	7.5	98.2	0.36
11	1999	Kocaeli, Turkey	Arcelik	523	Strike-slip	7.5	53.7	0.22
12	1992	Landers	Yermo Fire Station	354	Strike-slip	7.3	86	0.24
13	1992	Landers	Coolwater	271	Strike-slip	7.3	82.1	0.42
14	1989	Loma Prieta	Capitola	289	Strike-slip	6.9	9.8	0.53
15	1989	Loma Prieta	Gilroy Array #3	350	Strike-slip	6.9	31.4	0.56
16	1990	Manjil, Iran	Abbar	724	Strike-slip	7.4	40.4	0.51
17	1987	Superstition Hills	El Centro Imp. Co.	192	Strike-slip	6.5	35.8	0.36
18	1987	Superstition Hills	Poe Road (temp)	208	Strike-slip	6.5	11.2	0.45
19	1987	Superstition Hills	Westmorland Fire Stat.	194	Strike-slip	6.5	15.1	0.21
20	1992	Cape Mendocino	Rio Dell Overpass	312	Thrust	7.0	22.7	0.55
21	1999	Chi-Chi, Taiwan	CHY101	259	Thrust	7.6	32	0.44
22	1999	Chi-Chi, Taiwan	TCU045	705	Thrust	7.6	77.5	0.51
23	1971	San Fernando	LA - Hollywood Stor	316	Thrust	6.6	39.5	0.21
24	1976	Friuli, Italy	Tolmezzo	425	Thrust	6.5	20.2	0.35
25	1980	Irpinia	Bisaccia	496		6.9	21.3	0.94
26	1979	Montenegro	ST64	1083	Thrust	6.9	21.0	0.18
27	1997	Umbria Marche	ST238	n/a	Normal	6.0	21.5	0.19
28	2000	South Iceland	ST2487	n/a	Strike-slip	6.5	13	0.16
29	2000	South Iceland (a.s.)	ST2557	n/a	Strike-slip	6.5	15.0	0.13
30	2003	Bingol	ST539	806	Strike-slip	6.3	14.0	0.30

3.2   Intensity measure

The intensity scale factor, a_0, of both Eq.s (6) and (12) represents the seismic intensity measure (*IM*) in line with the performance-based earthquake engineering (PBEE) [50],[51]. In this study, the

abovementioned term is set equal to the spectral pseudo-acceleration, $S_A(T_d, \xi_d)$, corresponding to the isolated period of the bridge $T_d = 2\pi / \omega_d$ with the damping ratio $\Pi_{\xi_d} = \xi_d$. As also observed in [25]-[29], since the spectral acceleration is related to the spectral displacement $S_A(T_b, \xi_d) = \omega_d^2 S_d(T_d, \xi_d)$, if all the records are normalized with respect to $S_A(T_d, \xi_d)$, the normalized displacement and force of the isolated bridge deck, in the hypothesis of both a rigid substructure (pier) and absence of the sliding friction, are equal to 1 for each record without any record-to-record variability. Note that, in the following analyses, the damping ratio ξ_d is set equal to zero [25],[28],[37],[52] and the corresponding *IM* is hereinafter denoted to as $IM=a_0=S_A(T_d)$.

4 PARAMETRIC STUDY

In this study, the seismic performance of isolated bridges is assessed considering the effects of the higher order modes due to the flexibility of the elastic RC pier and also of the pier-abutment-deck interaction. This section describes the results of the parametric study carried out on the two systems of Fig. 1 to evaluate the performance of bridge isolated with FPS bearings for different structural properties. The first subsection deals with the response parameters relevant to the seismic performance, the second subsection reports the preliminary analysis for increasing dof in relation to the pier to demonstrate the effectiveness of the 6dof model in representing the bridge system response with and without the rigid RC abutment. The final subsection illustrates the parametric study results.

4.1 Non-dimensional response parameters relevant to the seismic performance assessment

The following response parameters relevant to the seismic performance assessment of isolated bridges are considered: the peak deck displacement relative to the pier for the model of Fig. 1(a) as well as the peak deck displacement relative to the pier or to the abutment for the model of Fig. 1(b), $u_{d,peak}$ (important for the design of both the FPS isolator and of the seismic joint deck-abutment), the peak pier displacement $u_{p,peak} = (\sum_{i=1}^{5} u_{p_i})_{peak}$ (related to the internal forces in the bridge substructure) for the both models. All these relevant response parameters can be defined in non-dimensional form, in line with Eq.s (6) and (12), as follows:

$$\psi_{u_d} = \frac{u_{d,peak} \omega_d^2}{a_0} \quad , \quad \psi_{u_p} = \frac{u_{p,peak} \omega_d^2}{a_0} = \frac{(\sum_{i=1}^{5} u_{p_i})_{peak} \omega_d^2}{a_0} \tag{15a,b}$$

Eq.s (6) and (12) are repeatedly and numerically solved in Matlab–Simulink [53] computing a set of samples for each response parameter for the two structural models. As also described in [25],[26],[28],[52],[54], the response parameters are modeled in probabilistic terms: the generic response parameter D (i.e., the extreme values ψ_{u_d}, ψ_{u_p} of Eq. (15)) can be fitted by a lognormal distribution estimating the sample geometric mean, $GM(D)$, and dispersion, $\beta(D)$, defined, respectively:

$$GM(D) = \sqrt[N]{d_1 \cdot ... \cdot d_N} \tag{16}$$

$$\beta(D) = \sigma_{\ln}(D) = \sqrt{\frac{(\ln d_1 - \ln[GM(D)])^2 + ... + (\ln d_N - \ln[GM(D)])^2}{N-1}} \tag{17}$$

in which d_h is the *h*-th sample realization of D, and N represents the total number of samples (i.e., ground motions): $h=1,...,N$. The *k*th percentile of the response parameter D can be evaluated as:

$$d_k = GM(D)\exp[f(k)\beta(D)] \tag{18}$$

where $f(k)$ is a function that assumes the following values $f(50)=0$, $f(84)=1$ and $f(16)=-1$ [55], for the 50th, 16th and 84th percentile, respectively.

4.2   Preliminary analysis for increasing dof with respect to the pier

This section describes a preliminary analysis with increasing dof in relation to the pier for the two structural configurations (i.e., single-column bent viaduct and multi-span continuous deck bridge). Specifically, the following mdof systems are compared: 2dof, 6dof and 8dof system (Fig.1(c)-(f)). For each mdof system, the first dof corresponds to the response of the deck whereas, the other degrees of freedom correspond to the different dof used to discretize the pier into a lumped mass system in order to take into account the effects of the higher order modes. In fact, although within the following parametric study, very low values of the vibration period of the pier are selected, a more accurate evaluation of the pier response needs a mdof system as also demonstrated in [29]. The following values have been considered: $T_p=0.2$s, $T_d=2$s and 4s, $\Pi_\lambda=0.2$, $\Pi_{\xi_p}=\xi_p=5\%$, $\Pi_{\xi_d}=\xi_d=0\%$ and

the normalised friction coefficient varying in the range: $\Pi_\mu^*=0,\dots,2$. Considering the presence of the abutment, the same FPS devices are assumed on the pier and on the abutment: $\Pi_{\mu p}^*=\Pi_{\mu a}^*=\Pi_\mu^*=0,\dots,2$.

In Fig.s 2-3, the median values of the normalized pier displacement are greater in the model with only pier, but with increasing values of the isolation period T_d, $GM(\psi_{u_p})$ decreases especially when the presence of the abutment is considered. As for the dispersion, the model which considers the pier-abutment-deck interaction presents higher values, and $\beta(\psi_{u_p})$ increases with increasing T_d.

With the increase of the degrees of freedom, $GM(\psi_{u_p})$ increases but $\beta(\psi_{u_p})$ generally decreases.
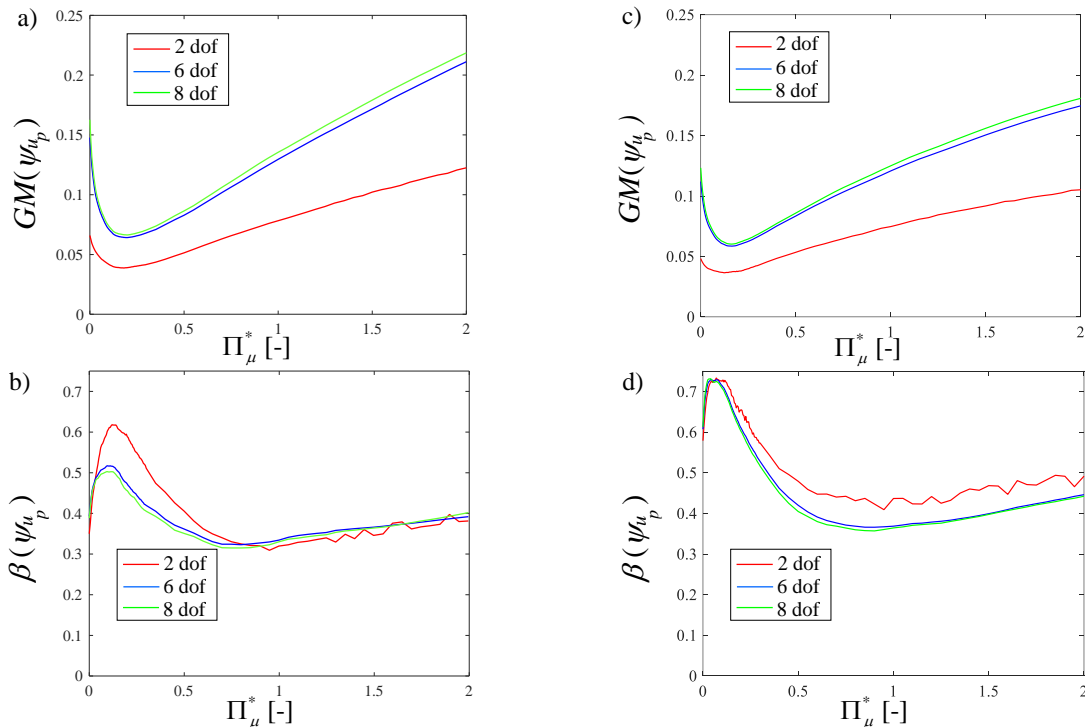

Fig. 2. Normalized pier displacement vs. Π^*_μ: median value ((a): analysis with only pier; (c): analysis with the pier-abutment-deck interaction) and dispersion ((b): analysis with only pier; (d): analysis with the pier-abutment-deck interaction) for $T_p=0.2$s, $\Pi_\lambda=0.2$ and $T_d=2$s.
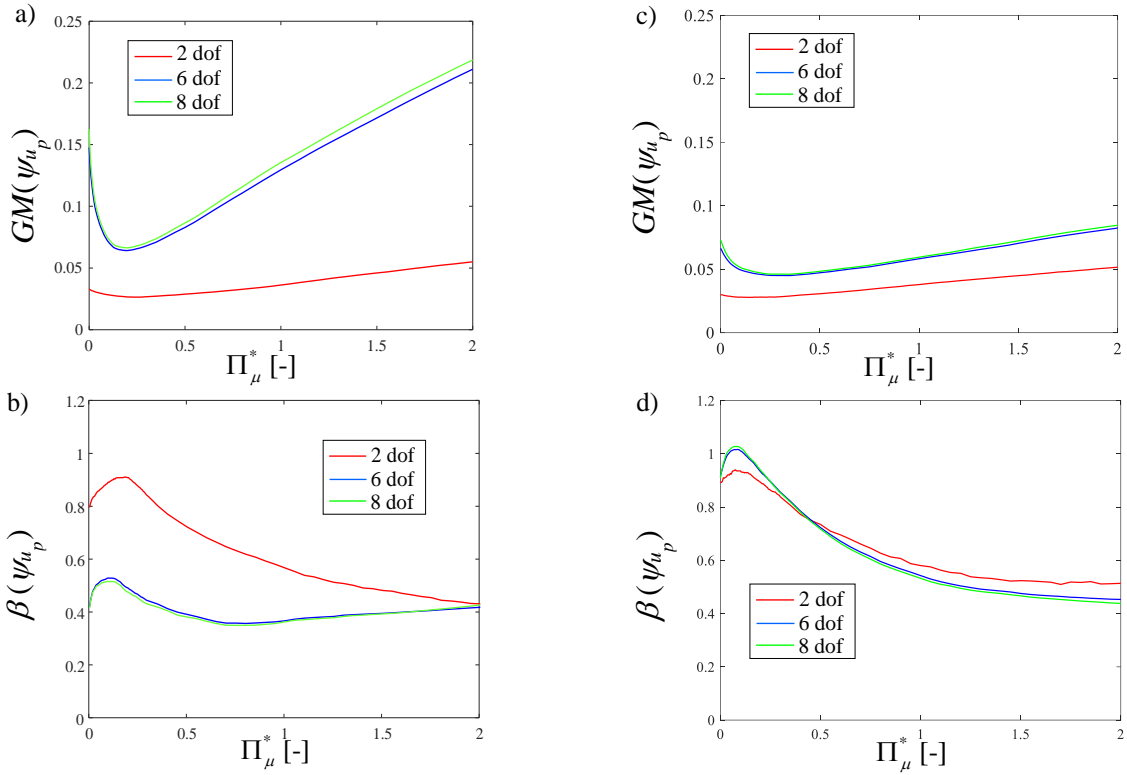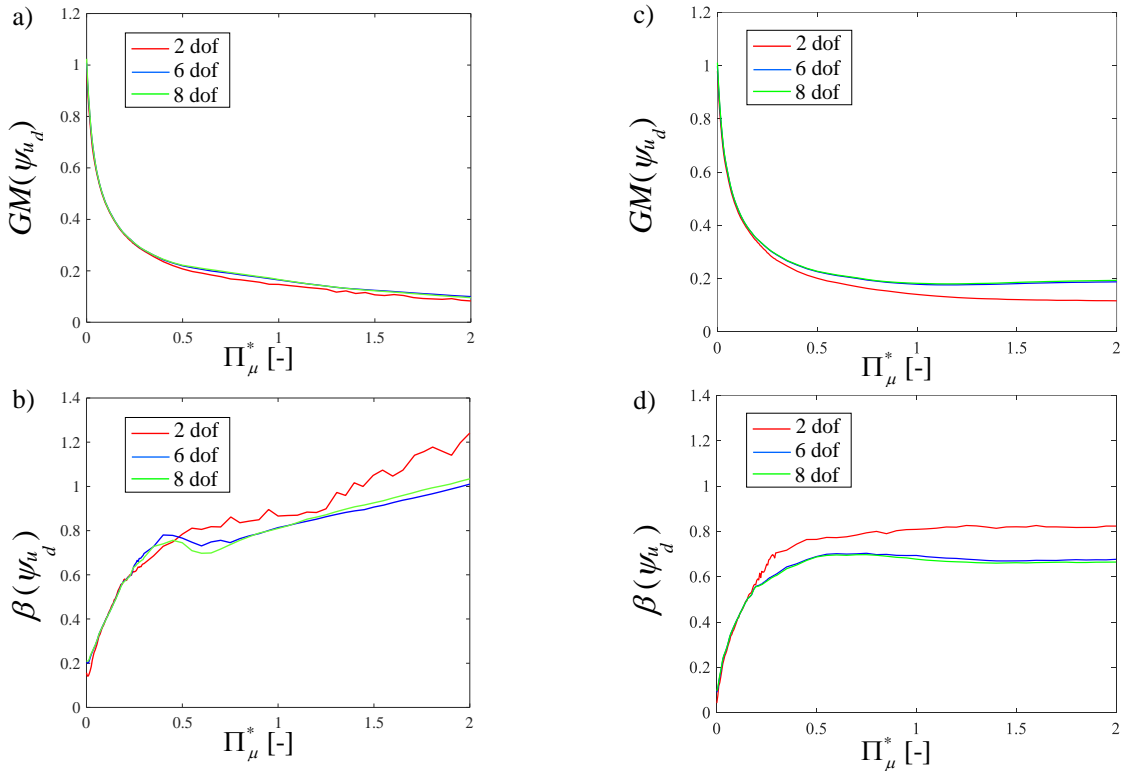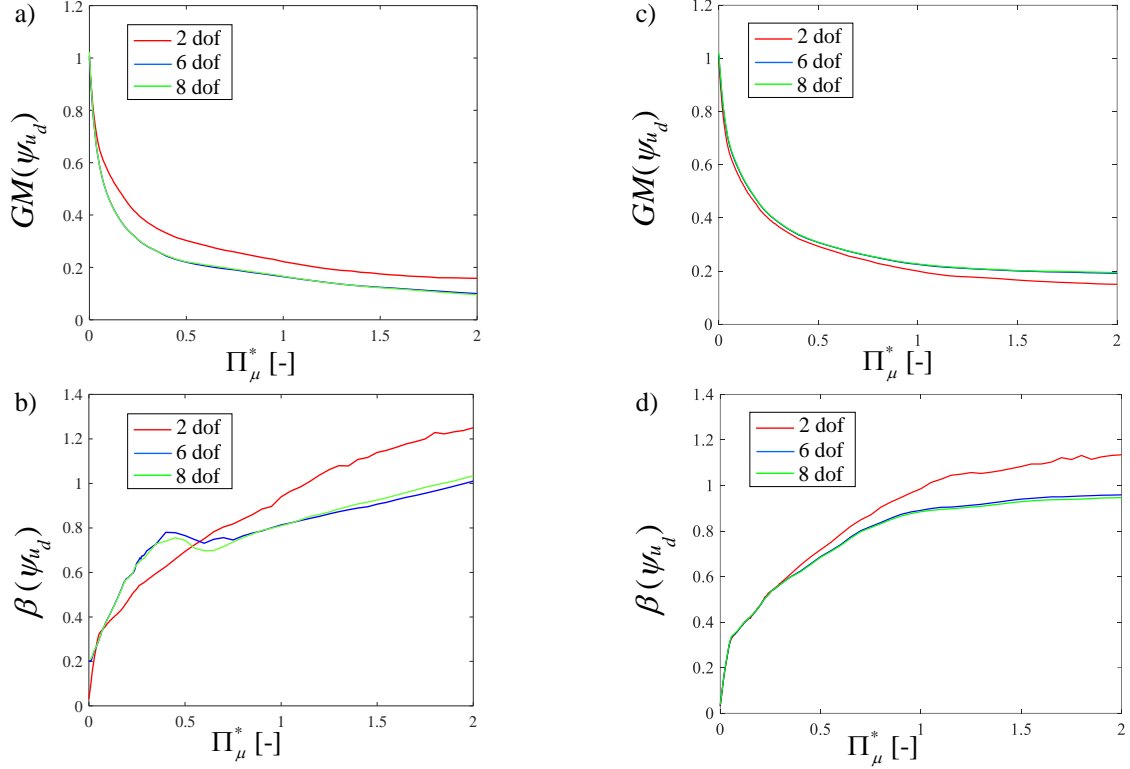
Fig. 3. Normalized pier displacement vs. Π^*_μ: median value ((a): analysis with only pier; (c): analysis with the pier-abutment-deck interaction) and dispersion ((b): analysis with only pier; (d): analysis with the pier-abutment-deck interaction) for T_p =0.2s, Π_λ=0.2 and T_d =4s.

Fig. 4. Normalized deck displacement vs. Π^*_μ: median value ((a): analysis with only pier; (c): analysis with the pier-abutment-deck interaction) and dispersion ((b): analysis with only pier; (d): analysis with the pier-abutment-deck interaction) for T_p =0.2s, Π_λ=0.2 and T_d =2s.

Fig. 5. Normalized deck displacement vs. Π^*_μ: median value ((a): analysis with only pier; (c): analysis with the pier-abutment-deck interaction) and dispersion ((b): analysis with only pier; (d): analysis with the pier-abutment-deck interaction) for T_p =0.2s, Π_λ=0.2 and T_d =4s.

In Fig.s 4-5, the median values of normalized deck displacement are greater in the configuration with the pier-abutment-deck interaction, and with the rise of the isolation period T_d, $GM\left(\psi_{u_d}\right)$ increases. As for the dispersion of normalized deck displacement: the model which considers only the pier is characterized by higher values, and $\beta\left(\psi_{u_d}\right)$ increases with increasing T_d. With the increase of the degrees of freedom, $GM\left(\psi_{u_d}\right)$ generally increases and $\beta\left(\psi_{u_d}\right)$ decreases.

The results have demonstrated the effectiveness of the 6dof systems for the both structural models since the results are very similar to the ones achieved for the 8dof systems. The choice of the 6dof systems represents a tradeoff between the computational effort and the accuracy of the results. Therefore, in the following parametric analysis the 6dof systems are employed for the two structural configurations (i.e., single-column bent viaduct and multi-span continuous deck bridge).

4.3   Comparison and parametric study: non-dimensional results

In this section, the results of the parametric study for the two structural configurations developed on the equivalent 6dof systems, for the different structural properties and 30 ground motion records, are illustrated and commented. Specifically, in line with [1],[10],[15],[32]-[33],[56]-[59], the parameters $\Pi_{\xi_d} = \xi_d$ and $\Pi_{\xi_p} = \xi_p$ are assumed respectively equal to 0% and 5%, the isolation period T_d varies in the range between 2s, 2.5s, 3s, 3.5s and 4s, the elastic RC pier period T_p from 0.05s to 0.2s with a step of 0.05s, $\Pi_\lambda = \lambda$ between 0.1, 0.15 and 0.2, Π_μ^* between 0 and 2. The latter one is related to the FPS device on the pier for the model without the abutment and to the FPS isolators, assumed equal, on the pier and on the abutment for the model of Fig. 1(b): $\Pi_{\mu p}^* = \Pi_{\mu a}^* = \Pi_\mu^*$. Indeed, high Π_μ^* values are considered to take also into account the very low values of the *IM* at very high isolated periods (i.e., T_d=4s) depending on the seismic hazard [60]. For each parameter combination and for

the two structural configurations, the differential motion equations (Eq.s (6) and (12)) have been repeatedly and numerically solved adopting the Bogacki-Shampine and Runge-Kutta-Fehlberg integration algorithm available in Matlab-Simulink [53]. After that, for each normalized response parameter, the geometric mean, GM, and the dispersion, β, have been evaluated by means of Eq.s (16) and (17) and are illustrated in Fig.s 6-13 for the both structural models. Each figure contains different meshes as many as the values of Π_λ: the arrow indicates the increasing values of Π_λ.

Note that for the configuration with the pier-abutment-deck interaction (i.e., multi-span continuous deck bridge), the peak normalized deck displacement, showed in Fig.s 6-9, has always been the one between the deck and the abutment. This is because of the elastic response of the pier that reduces the relative displacement between the deck and itself.

In Fig.s 6-9, $GM\left(\psi_{u_d}\right)$ is quite perfectly equal to unit for $\Pi_\mu^* = 0$ and $T_p = 0.05$s because of the very reduced influence of the pier behaviour. For $\Pi_\mu^* \neq 0$, $GM\left(\psi_{u_d}\right)$ increases slightly for increasing T_d because of the period elongation. Obviously, $GM\left(\psi_{u_d}\right)$ decreases significantly as Π_μ^* increases showing an hyperbolic trend while it is not heavily influenced by Π_λ. The dispersion $\beta\left(\psi_{u_d}\right)$, for high T_d, increases for increasing values of Π_μ^*, as a result of the reduction of the efficiency of the *IM*.
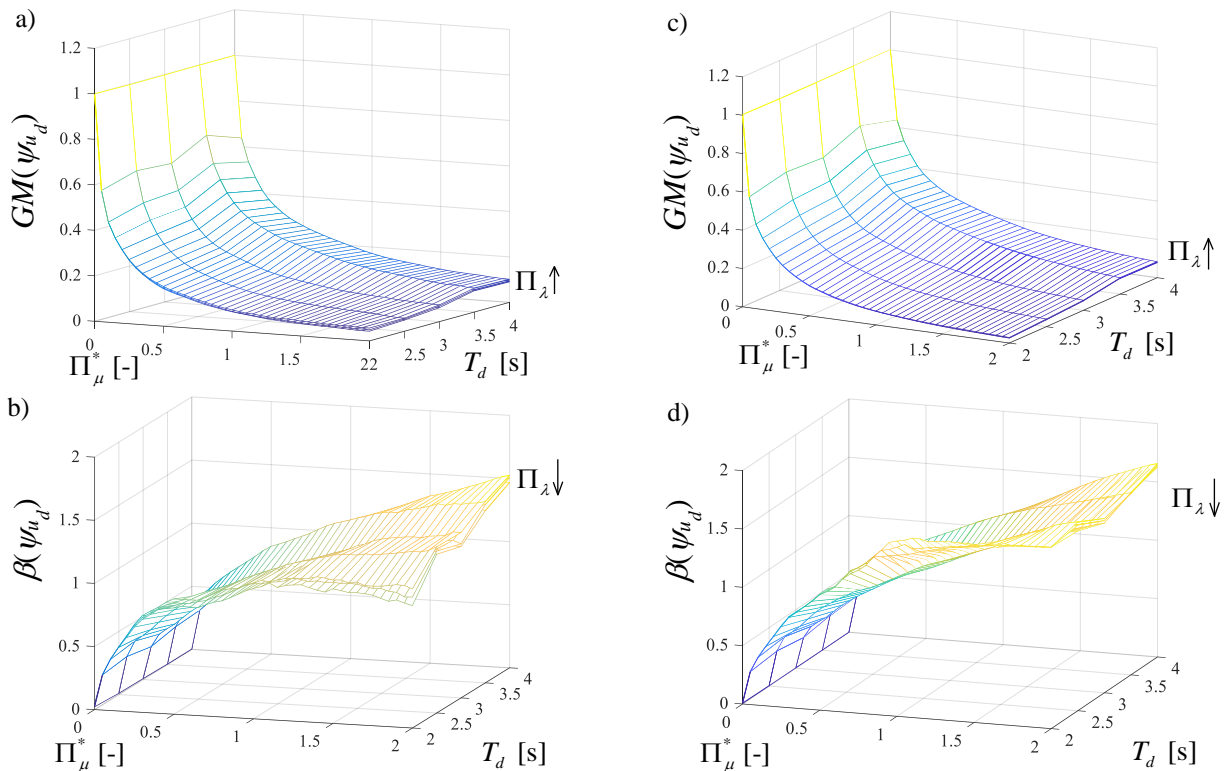

Fig. 6. Normalized deck displacement vs. Π_μ^* and T_d: median value ((a): analysis with only pier; (c): analysis with the pier-abutment-deck interaction) and dispersion ((b): analysis with only pier; (d): analysis with the pier-abutment-deck interaction) for $T_p = 0.05$s and for different values of Π_λ.
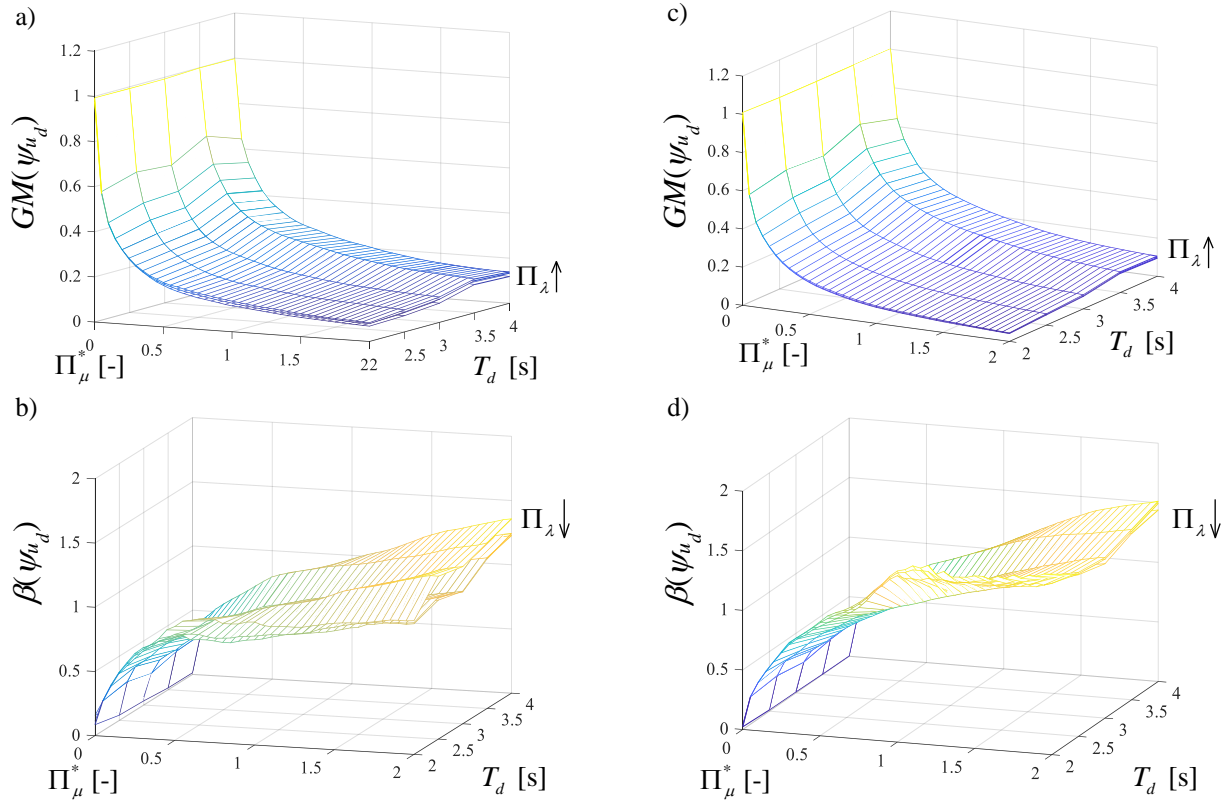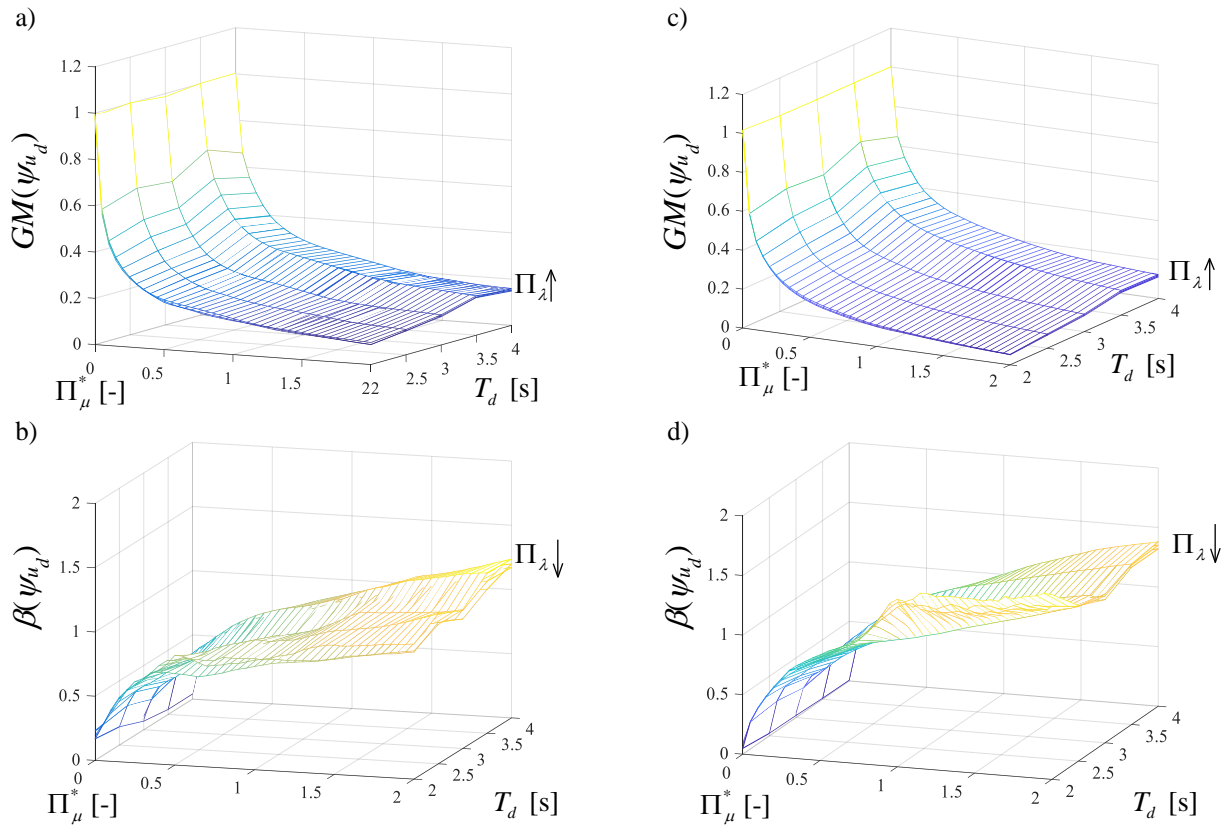
Fig. 7. Normalized deck displacement vs. Π^*_μ and T_d: median value ((a): analysis with only pier; (c): analysis with the pier-abutment-deck interaction) and dispersion ((b): analysis with only pier; (d): analysis with the pier-abutment-deck interaction) for T_p =0.1s and for different values of Π_λ.
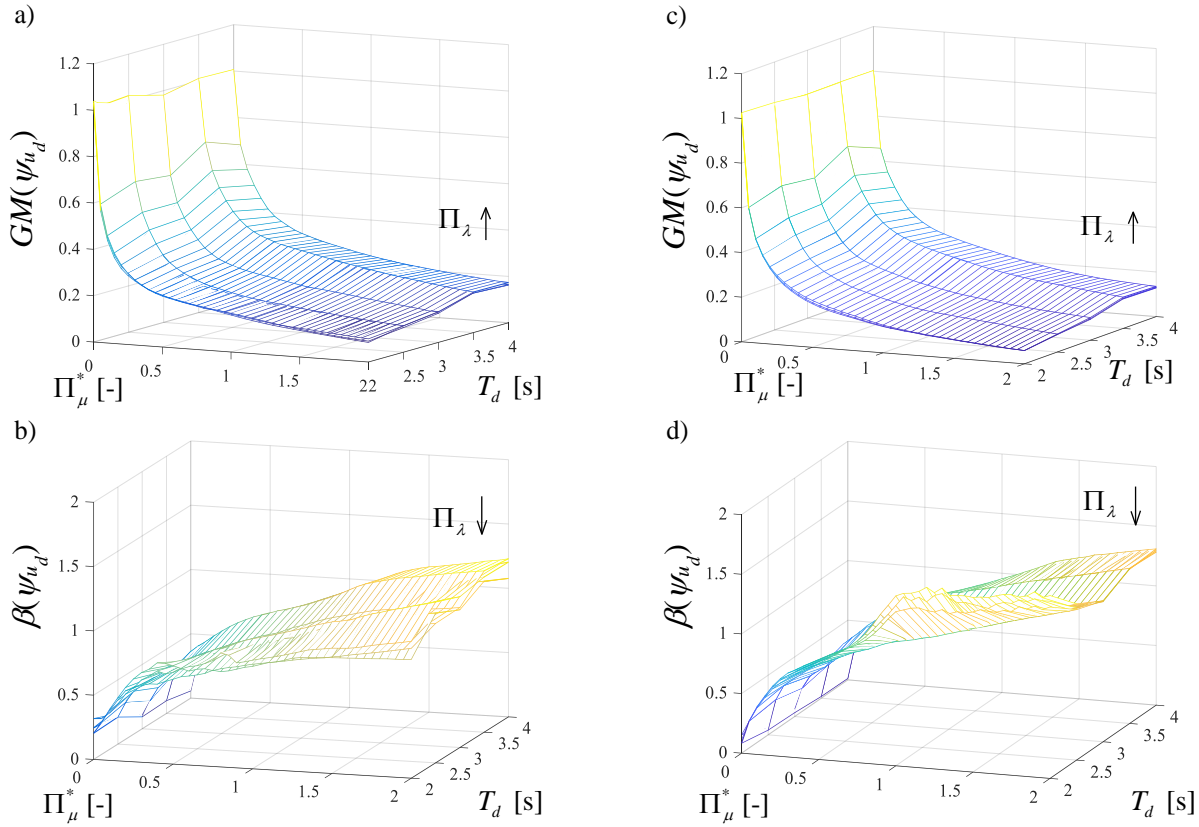

Fig. 8. Normalized deck displacement vs. Π^*_μ and T_d: median value ((a): analysis with only pier; (c): analysis with the pier-abutment-deck interaction) and dispersion ((b): analysis with only pier; (d): analysis with the pier-abutment-deck interaction) for T_p =0.15s and for different values of Π_λ.
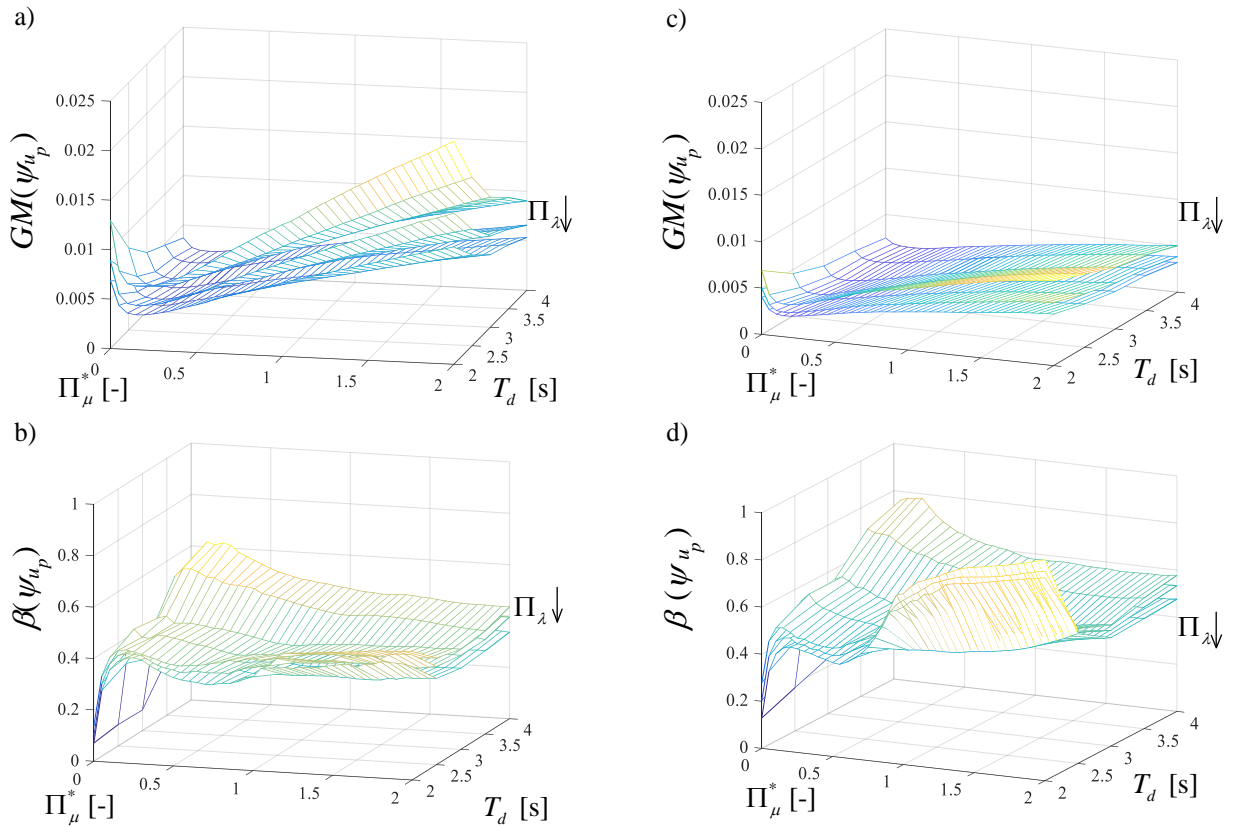
Fig. 9. Normalized deck displacement vs. Π^*_μ and T_d: median value ((a): analysis with only pier; (c): analysis with the pier-abutment-deck interaction) and dispersion ((b): analysis with only pier; (d): analysis with the pier-abutment-deck interaction) for T_p =0.2s and for different values of Π_λ.
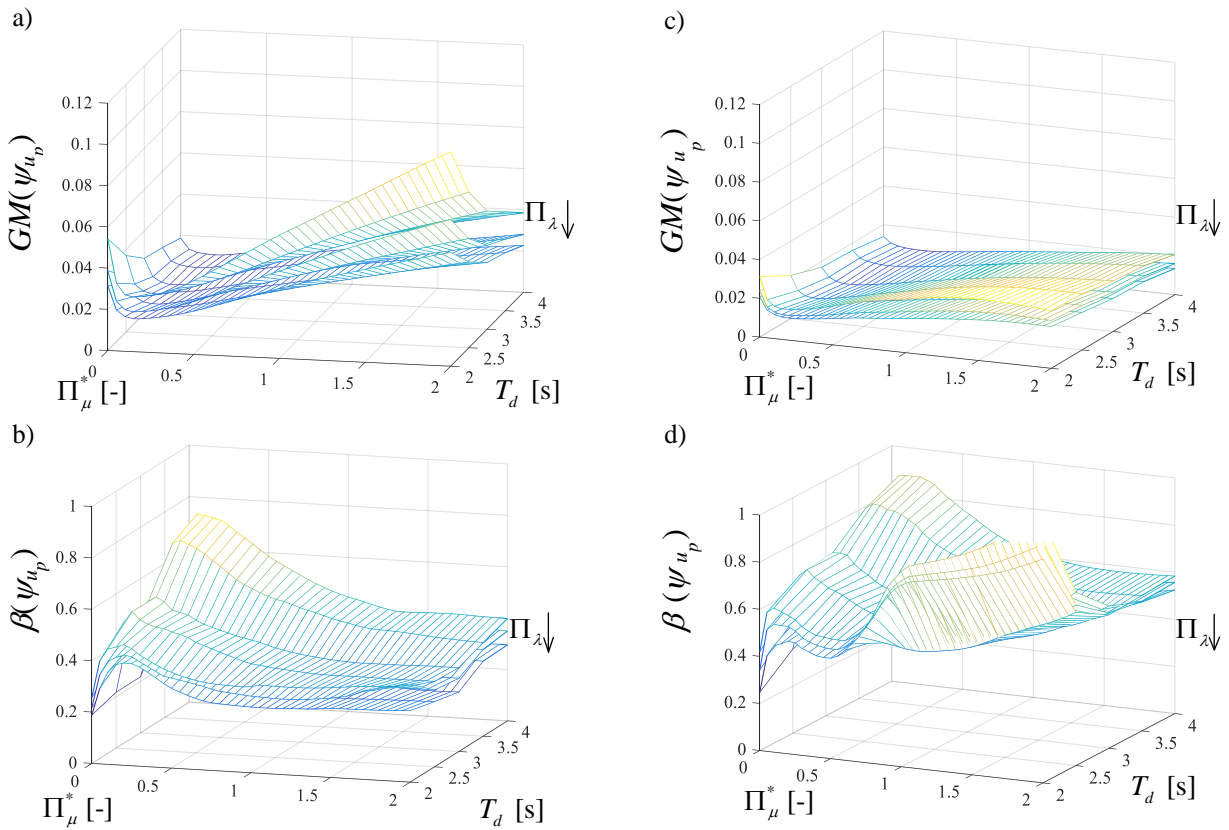

Fig. 10. Normalized pier displacement vs. Π^*_μ and T_d: median value ((a): analysis with only pier; (c): analysis with the pier-abutment-deck interaction) and dispersion ((b): analysis with only pier; (d): analysis with the pier-abutment-deck interaction) for T_p =0.05s and for different values of Π_λ.

Fig. 11. Normalized pier displacement vs. Π^*_μ and T_d: median value ((a): analysis with only pier; (c): analysis with the pier-abutment-deck interaction) and dispersion ((b): analysis with only pier; (d): analysis with the pier-abutment-deck interaction) for $T_p =0.1$s and for different values of Π_λ.
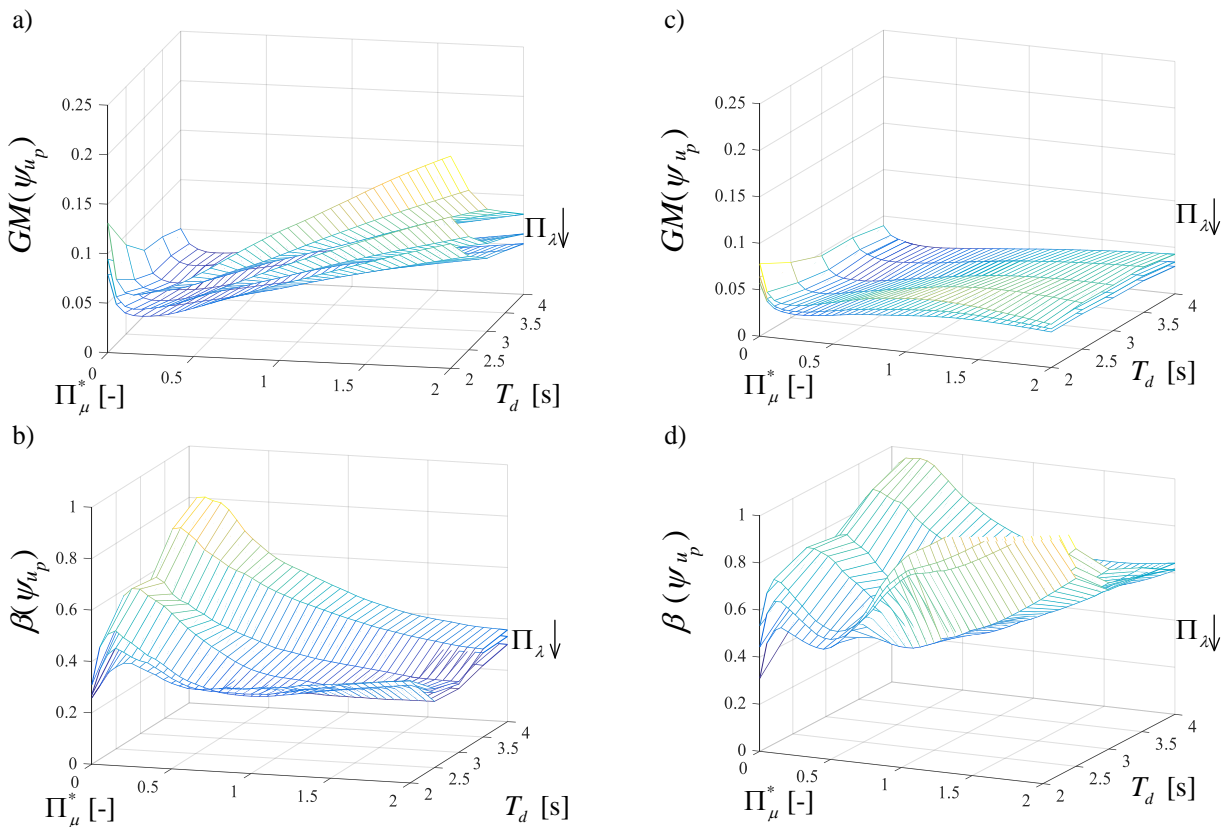

Fig. 12. Normalized pier displacement vs. Π^*_μ and T_d: median value ((a): analysis with only pier; (c): analysis with the pier-abutment-deck interaction) and dispersion ((b): analysis with only pier; (d): analysis with the pier-abutment-deck interaction) for $T_p =0.15$s and for different values of Π_λ.
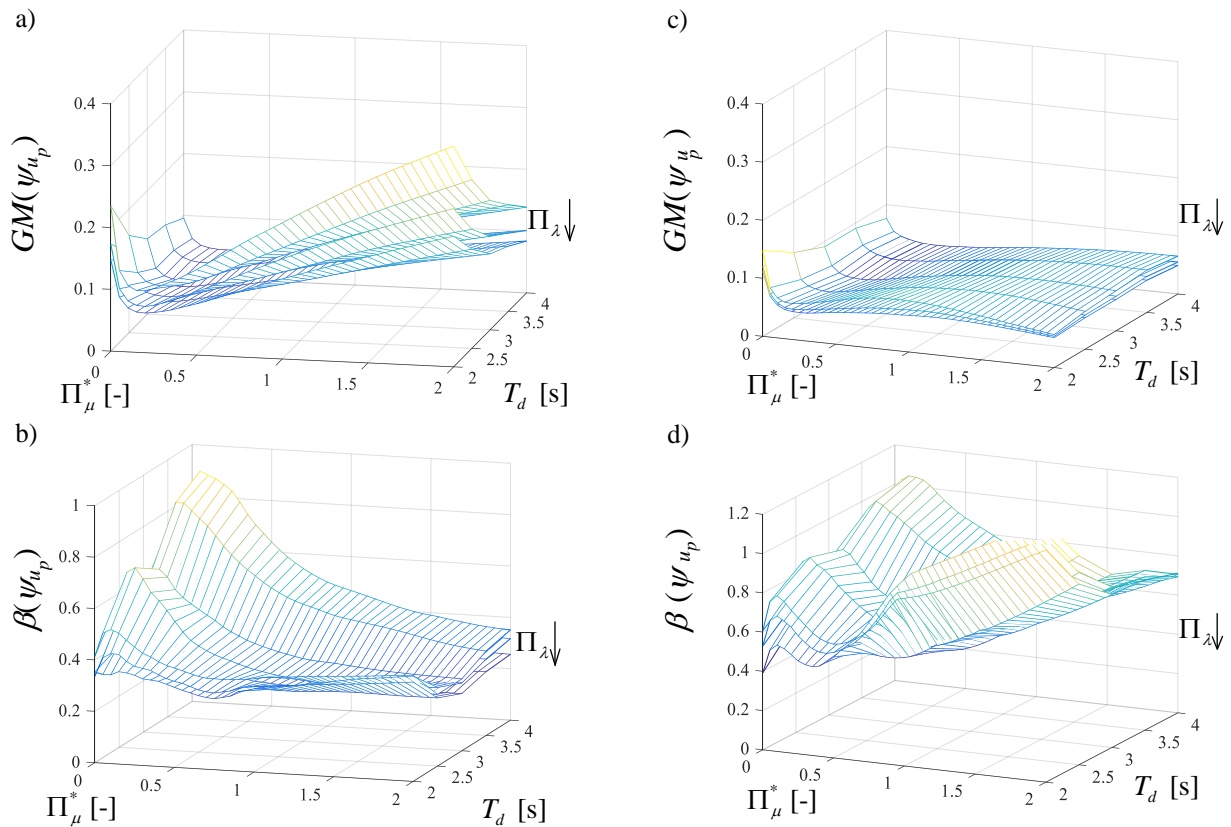
Fig. 13. Normalized pier displacement vs. Π^*_μ and T_d: median value ((a): analysis with only pier; (c): analysis with the pier-abutment-deck interaction) and dispersion ((b): analysis with only pier; (d): analysis with the pier-abutment-deck interaction) for T_p =0.2s and for different values of Π_λ.

Obviously, in the reference situation corresponding to $\Pi^*_\mu = 0$ and T_p =0.05s, the dispersion is zero for all the values of T_d and of Π_λ considered. The mass ratio Π_λ does not affect significantly the response dispersion, especially in the case of high T_p values. Although the trends of the both statistics are similar for the two configurations, it is possible to observe that the values of $GM\left(\psi_{u_d}\right)$ are larger in the case of the model without the pier-abutment-deck interaction. Differently, higher values of $\beta\left(\psi_{u_d}\right)$ are achieved for the model with the pier-abutment-deck interaction.

Fig.s 10-13 show the response statistics of the normalized pier displacement ψ_{u_p}. For the both structural configurations, $GM\left(\psi_{u_p}\right)$ decreases for higher values of T_d and of Π_λ as well as for decreasing values of T_p; whereas it first decreases and then increases for increasing values of Π^*_μ. It follows that there is an optimal value of Π^*_μ able to minimize the geometric mean of the pier displacement. This optimal value varies in a range that depends on the values of T_p, T_d, Π_λ and on the structural configuration. In fact, as can be observed, the sagging zones of the meshes related to the case with the pier-abutment-deck interaction (i.e., multi-span continuous deck bridge) are larger, leading to higher values of these optimal ranges. This happens because the seismic device on the pier slides with a velocity lower than the one of the device on the abutment. Note also that for not optimal values of Π^*_μ, $GM\left(\psi_{u_p}\right)$ is not so high. Conversely, $GM\left(\psi_{u_p}\right)$ presents higher values for the structural configuration without the pier-abutment-deck interaction (i.e., single-column bent viaduct). The values of the dispersion $\beta\left(\psi_{u_p}\right)$ are very low for low Π^*_μ values due to the high efficiency of

the *IM* used in this work, and attain their peak for values of Π_μ^* close to the optimal ones. The other system parameters have a reduced influence on $\beta\left(\psi_{u_p}\right)$ compared to the influence of Π_μ^*. Higher values are achieved for the structural configuration with the pier-abutment-deck interaction (i.e., multi-span continuous deck bridge).

As observed in similar studies [25]-[29],[61]-[64], the existence of an optimal value of the friction coefficient derives from a combination of three effects depending on the value of the sliding friction coefficient: the dissipated energy, the isolator forces and displacements demand.

5   OPTIMAL VALUES OF THE SLIDING FRICTION COEFFICIENTS WITH REGRESSION ANALYSIS

From the results defined in the previous section, for each parameter combination (i.e., Π_λ, T_d and T_p) and structural model (i.e., single-column bent viaduct and multi-span continuous deck bridge), the optimal values of the normalized sliding friction coefficient, $\Pi_{\mu,\text{opt}}^*$, that minimize the median (50$^{\text{th}}$ percentile) normalized pier displacements ψ_{u_p} have been computed and are reported in Fig. 14. Minimizing the pier displacements relative to the ground represents a notable design requirement for the safety of bridges in order to assure an adequate seismic protection and avoid any inelastic response. Fig. 14 reports the variation of $\Pi_{\mu,\text{opt}}^*$ with Π_λ and T_p for each T_d and in relation to the two structural models (Fig. 14a,b,c,d,e -1-2). According to [9], the optimal values of the sliding friction coefficient slightly increase for decreasing T_d, especially for low T_p, and this is valid for the both configurations. It is also observed that, especially for high T_d values, $\Pi_{\mu,\text{opt}}^*$ increases by increasing Π_λ and T_p to dissipate more energy and the friction coefficient attains its peak when all the three parameters (i.e., T_d, T_p and Π_λ) are considered with their maximum values together.
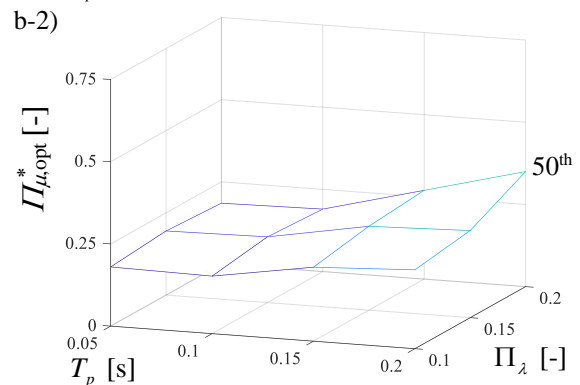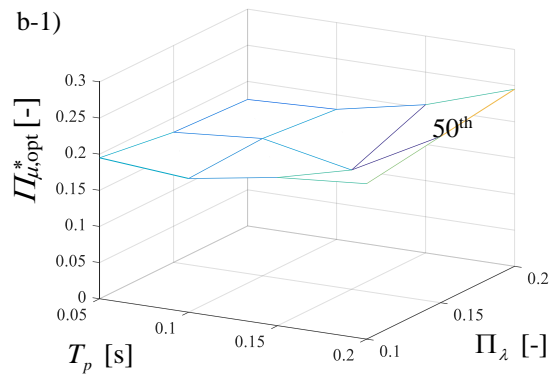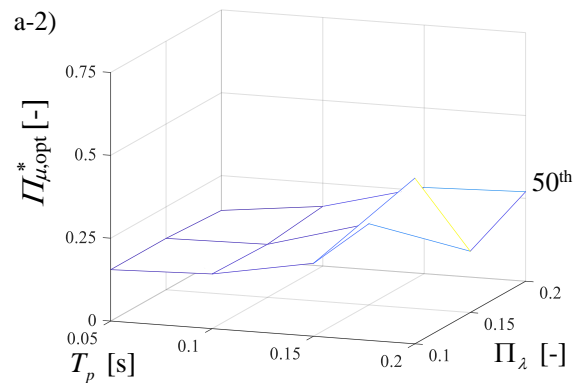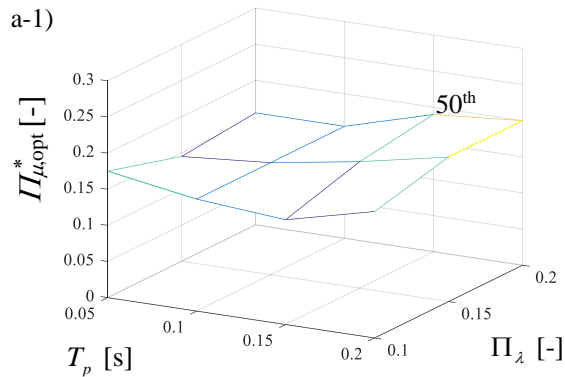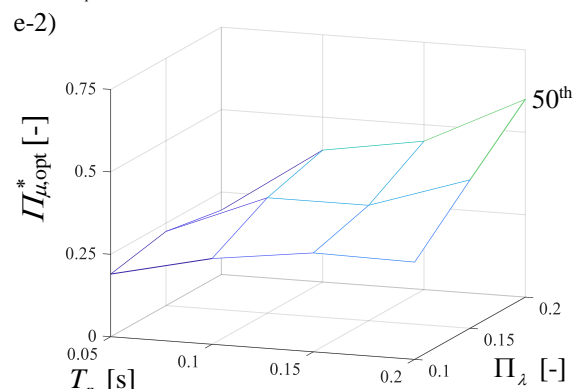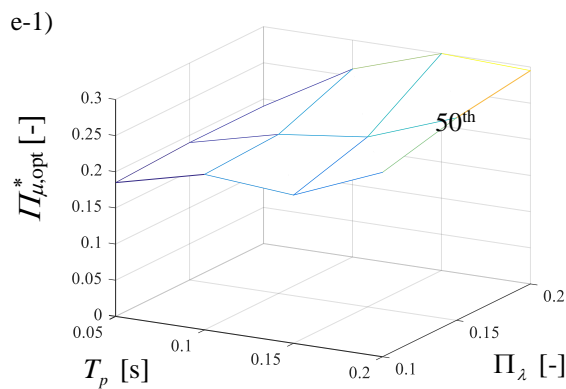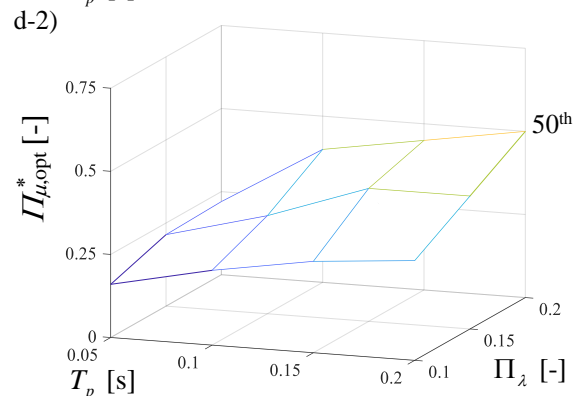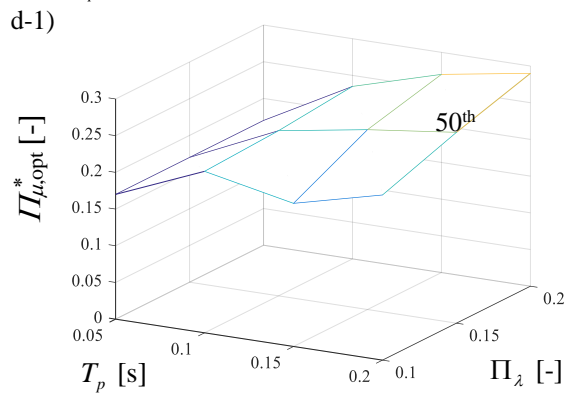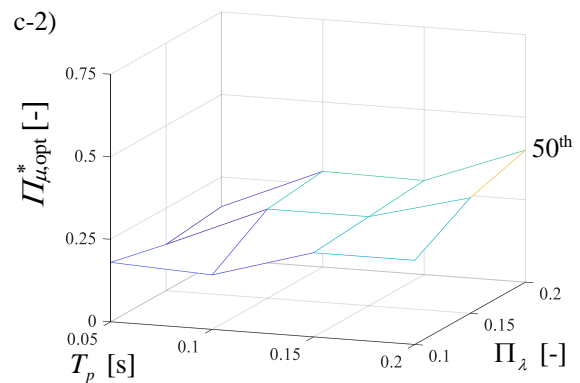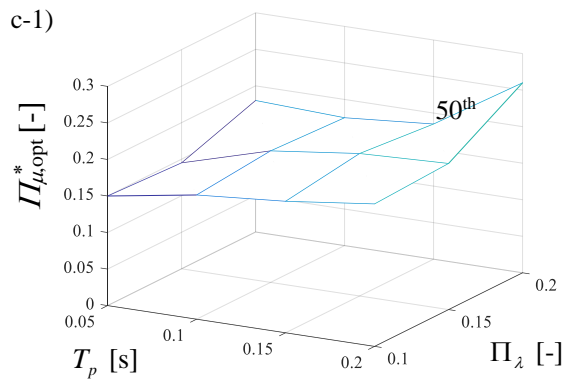
Fig. 14. Optimal values of normalized friction that minimize the 50th percentile of the normalized pier displacements vs. Π_λ and T_p, for T_d =2s (a), T_d =2.5s (b), T_d =3s (c), T_d =3.5s (d) and T_d =4s (e). The column-1 reports the analysis with only pier; the column-2 reports the results for the analysis with the pier-abutment-deck interaction.
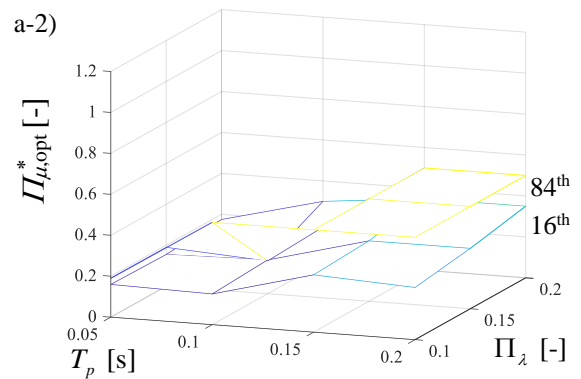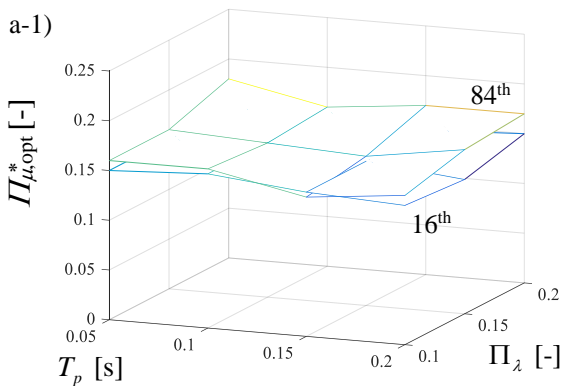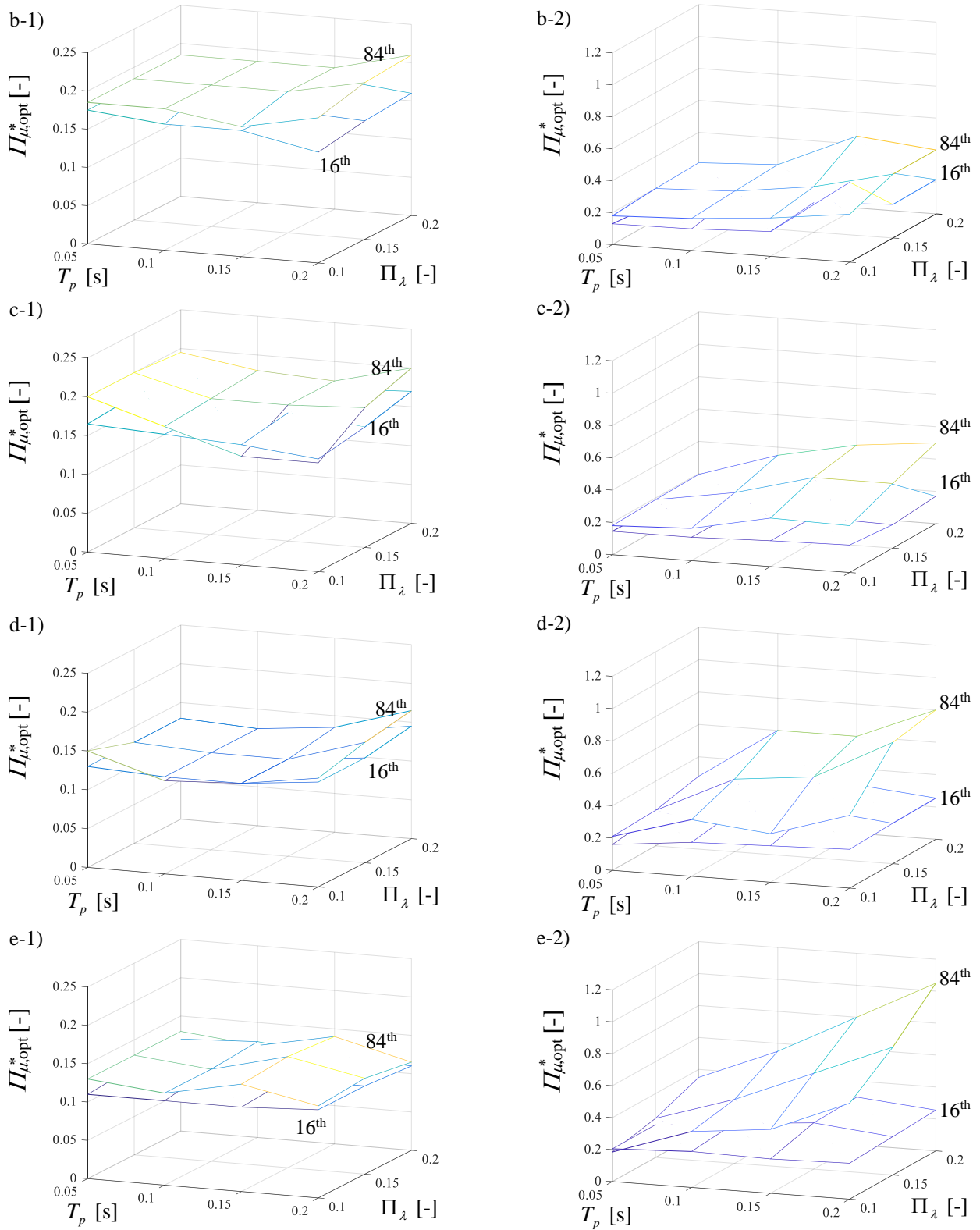
Fig. 15. Optimal values of normalized friction that minimize the 84th and 16th percentiles of the normalized pier displacements vs. Π_λ and T_p, for T_d =2s (a), T_d =2.5s (b), T_d =3s (c), T_d =3.5s (d) and T_d =4s (e). Column-1 reports the analysis with only pier; column-2 reports the results for the analysis with the pier-abutment-deck interaction.

Between the two configurations, it is possible to see that for the model with pier-abutment-deck interaction (i.e., multi-span continuous deck bridge), the values of $\Pi^*_{\mu,\mathrm{opt}}$ are higher than the ones of

the other model (i.e., single-column bent viaduct). This result is in compliance with the responses previously obtained when the pier-abutment-deck interaction is considered.

In order to assure a higher safety level, it might be of interest to define the values of $\Pi^*_{\mu,\mathrm{opt}}$ that minimize others response percentiles [52]. Fig. 15 shows the optimal values of the normalized friction coefficients that minimize the 84th and 16th percentiles of the normalized pier response for the different values of Π_λ, T_p, T_d regarding the two structural models (Fig. 15 a,b,c,d,e -1-2). In the case of the only pier model (i.e., single-column bent viaduct), $\Pi^*_{\mu,\mathrm{opt}}$ is not significantly affected by neither T_p nor Π_λ, for both the percentiles. In the case of the pier-abutment-deck interaction (i.e., multi-span continuous deck bridge), the optimal coefficient of friction able to minimize the 84th percentile of the response tends to increase when increasing values of Π_λ are considered, especially for higher values of the isolation period T_d. On the other hand, as for the 16th percentile of the normalized pier response, the meshes show a more constant trend with respect to both T_p and Π_λ. In terms of magnitude, the comparison between the two models shows higher values for the optimal normalized friction coefficient useful to minimize each percentile of the response, when the pier-abutment-deck interaction is considered (i.e., multi-span continuous deck bridge), and this is as more relevant for higher values of T_d.

Through a multivariate nonlinear regression analysis, expressions are obtained for estimating $\Pi^*_{\mu,\mathrm{opt}}$ and ψ_{up} as a function of the structural properties Π_λ, T_d, T_p and of the percentile level (i.e., 50th, 16th and 84th) for the both structural models. The expressions for $\Pi^*_{\mu,\mathrm{opt}}$ and ψ_{up} are derived by fitting in Matlab [53], respectively, the following second-order polynomial expressions:

$$\Pi^*_{\mu,opt} = c_1 + c_2 T_p + c_3 T_d + c_4 \Pi_\lambda + c_5 T_p T_d + c_6 T_p \Pi_\lambda + c_7 \Pi_\lambda T_d + c_8 T_p^2 + c_9 T_d^2 + c_{10} \Pi_\lambda^2 \tag{19}$$

$$\psi_{up} = c_1 + c_2 T_p + c_3 T_d + c_4 \Pi_\lambda + c_5 T_p T_d + c_6 T_p \Pi_\lambda + c_7 \Pi_\lambda T_d + c_8 T_p^2 + c_9 T_d^2 + c_{10} \Pi_\lambda^2 \tag{20}$$

In Eq.s (19) and (20), c_i, i=1,…,10, are the regression coefficients, whose values are reported in Tables 2-5, respectively, as a function of the different percentile levels and for the two models (i.e., single-column bent viaduct and multi-span continuous deck bridge). It is noteworthy that simple polynomial expressions have been adopted for a preliminary design of the FPS characteristics and a preliminary definition of the peak displacement of the pier.

Eq. (19) can be used to design the optimum FPS properties for isolated bridges in order to reduce a percentile of the response as a function of the safety level required and given an *IM* level $S_A(T_d)$ corresponding to a seismic ultimate limit state [60] (i.e., near-collapse limit state). In fact, according to Eq.s (8) and (14), the non-normalized optimum friction coefficient (at high velocity) can be easily calculated for the device on the pier and/or on the abutment as $\mu_{\mathrm{max,opt}} = \dfrac{\Pi^*_{\mu,\mathrm{opt}} \cdot S_A(T_d)}{g}$. This means that the (non-normalized) optimum friction coefficient increases linearly with the *IM* level and so depends on the seismic intensities corresponding to the limit states. The regression R-squared value is higher than about 0.93 for the model with the pier-abutment-deck interaction. For the other model, R-squared value is higher than 0.90 for the 50th percentile whereas for the other two percentiles R-squared value is higher than 0.7.

Eq. (20) can be used to estimate the peak pier's displacement for isolated bridges depending on the seismic intensity level $S_A(T_d)$ as shown by Eq. (15(b)). In this way, it can be easily calculated as

$$u_{p,peak} = \frac{\psi_{u_p} S_A(T_d)}{\omega_d^2}$$. Similarly to $\mu_{max,opt}$, $u_{p,peak}$ increases linearly with the *IM* level and depends on the seismic intensities, too. The regression R-squared value is higher than about 0.96 for the both structural configurations.

Table 2. Coefficients of multi-variate non-linear regression - $\Pi^*_{\mu,opt}$ (structural model with pier-abutment-deck interaction).

	c_1	c_2	c_3	c_4	c_5	c_6	c_7	c_8	c_9	c_{10}
50th percentile	0.6504	-0.1530	-0.2512	-3.0175	0.2160	5.7600	1.0025	-0.6333	0.0229	0.1000
84th percentile	1.1202	-3.3907	-0.5135	-3.6625	1.3280	12.3000	1.1825	-1.7667	0.0533	0.9500
16th percentile	6.0058	24.7573	-3.6519	-19.5525	-6.0040	-12.2400	2.9325	-4.8000	0.5910	35.8000

Table 3. Coefficients of multi-variate non-linear regression - ψ_{up} (structural model with pier-abutment-deck interaction).

	c_1	c_2	c_3	c_4	c_5	c_6	c_7	c_8	c_9	c_{10}
50th percentile	0.0280	0.1813	-0.0157	-0.1376	-0.0378	-0.3327	0.0267	1.0472	0.0022	0.2258
84th percentile	0.0499	0.1720	-0.0300	-0.1769	-0.0463	-0.1329	0.0342	2.1290	0.0045	0.2411
16th percentile	-0.0076	0.0785	0.0069	-0.0371	0.0006	-0.1652	0.0002	0.2391	-0.0014	0.1225

Table 4. Coefficients of multi-variate non-linear regression - $\Pi^*_{\mu,opt}$ (structural model with only pier).

	c_1	c_2	c_3	c_4	c_5	c_6	c_7	c_8	c_9	c_{10}
50th percentile	0.3332	-0.7983	-0.0561	-1.2850	0.1833	3.4000	0.2100	0.5666	0.0056	1.6000
84th percentile	0.5089	-2.3606	-0.1615	-1.5625	0.6066	7.5400	0.4025	1.4333	0.0162	0.5500
16th percentile	0.4750	-0.7423	-0.1696	-0.5075	0.1707	2.4200	0.3025	-0.4667	0.0209	-2.3499

Table 5. Coefficients of multi-variate non-linear regression - ψ_{up} (structural model with only pier).

	c_1	c_2	c_3	c_4	c_5	c_6	c_7	c_8	c_9	c_{10}
50th percentile	0.0609	0.5394	-0.0328	-0.3743	-0.1093	-1.1436	0.0664	1.2904	0.0046	0.7472
84th percentile	0.0976	0.5598	-0.0519	-0.5027	-0.1137	-0.9082	0.8677	2.0739	0.0072	0.8888
16th percentile	0.0374	0.4756	-0.0204	-0.2818	-0.0944	-1.0857	0.0524	0.7358	0.0029	0.5901

These two nondimensional regressions, useful for the preliminary design or retrofit of both single-column bent viaducts and multi-span continuous deck bridges located in any site and in relation, especially, to the seismic ultimate limit states for the non-frequent ground motions selected, can be used as follows. Known the geometry and dynamic characteristics (i.e., Π_λ , T_d , T_p) of the structural system, fixed a seismic ultimate limit state according to the location and code and considering, especially, the 50th or 84th percentiles, Eq.(19) can be employed and consequently $\mu_{max,opt}$ can be computed. After that, considering the same percentile, Eq.(20) can be employed and consequently $u_{p,peak}$ can be computed. Successively, within the same percentile and for the optimal value $\Pi^*_{\mu,opt}$ previously achieved, the non-dimensional results in Fig.s 6-9 together with Eq.(18) can be used to estimate the nondimensional seismic demand to the deck and isolators, and consequently $$u_{d,peak} = \frac{\psi_{u_d} S_A(T_d)}{\omega_d^2}$$ can be computed. In this way, it is possible to achieve the design information with respect to the FPS isolators, pier, deck and seismic joint deck-abutment.

Finally, it is also worth underlining that the optimal properties of the FPS devices have been estimated considering only the seismic loads, but during the design phase of bridges, other serviceability actions such as thermal movements [65] have to be absolutely considered. These factors, in fact, can influence the design and the costs of piers and of foundations when high values of the fiction coefficient are necessary under earthquake events. For these situations, a cost-effectiveness analysis considering all

the different actions could be useful to reduce the construction costs provided that the same safety level is assured. Moreover, the deterioration of the sliding surface of the isolator can be taken into account by means of the property modification factors, as discussed in [66].

6 CONCLUSIONS

This paper describes the seismic performance of bridges and viaducts isolated with single concave friction pendulum system bearings in order to evaluate the influence of the pier-abutment-deck interaction and define the optimal isolator friction properties taking into account the uncertainty in the seismic input. By means of a nondimensionalization of the motion equations with respect to the seismic intensity, a wide parametric analysis for several structural properties has been carried out by monitoring the response parameters of interest regarding both an isolated bridge where only the pier response is considered and an isolated bridge where the interaction between pier and abutment is taking into account (i.e., single-column bent viaduct and multi-span continuous deck bridge, respectively). The behavior of these systems is modelled by employing a six-degree-of-freedom system accounting for the effects due to the higher modes of the elastic pier. A preliminary analysis among a 2dof, 6dof and 8dof model has also been illustrated to demonstrate that the equivalent 6dof model is very effective in estimating the deck and pier response for the both structural configurations. With reference to the deck response, the geometric mean of the normalized deck displacement increases slightly for increasing isolation period because of the period elongation and it decreases significantly as the normalized friction increases. The dispersion increases for increasing both isolation period and normalised friction coefficient. The other structural parameters do not significantly affect the deck response statistics. Regarding the model accounting for the pier-abutment-deck interaction (i.e., multi-span continuous deck bridge), the geometric mean of the normalized deck displacement tends to be lower than the outcomes of the model with only pier (i.e., single-column bent viaduct). An opposite result is obtained regarding the dispersion.

With reference to the pier response, the geometric mean of the normalized displacement decreases for increasing values of isolation period and of mass ratio as well as for decreasing values of pier period, whereas it first decreases and then increases for increasing values of normalized friction. Thus, there exists an optimal value of normalized friction coefficient such that the pier displacement is minimized. This optimal value varies in the range between 0.1 and 0.3 depending on the other system properties. The opposite trend is observed for the dispersion that increases for increasing values of both the pier period and isolation period and for decreasing values of the mass ratio. In the case of pier-abutment-deck interaction model (i.e., multi-span continuous deck bridge), lower values of the geometric mean are observed for any pier's period with a reduced influence of both the isolation period and the mass ratio; higher values of the optimal normalised friction coefficient are required to minimize any response percentile. Regarding the dispersion, higher values are observed for the pier-abutment-deck interaction model. This happens because the seismic device on the pier slides with a velocity lower than the one of the device on the abutment.

Finally, multi-variate regression expressions are defined in order to estimate the optimal values of the normalized friction coefficient able to minimize the 50th, 16th and 84th percentiles of the pier response, as a function of the structural properties and for the both structural models herein investigated. Higher optimum friction coefficients are required, when the pier-abutment-deck interaction (i.e., multi-span continuous deck bridge) is taken into account. Furthermore, when all the structural parameters Π_λ, T_p, T_d are picked with their maximum values, larger values of the optimum friction coefficient are required to increase the energy dissipation. Furthermore, note that friction pendulum properties that are "optimal" for a given seismic intensity, are not "optimal" for the other intensities corresponding to other sites and limit states. In addition, a regression expression is also provided to estimate the corresponding response of the pier.

These proposed nondimensional regressions can be very useful for the preliminary design or retrofit of both single-column bent viaducts and multi-span continuous deck bridges with the scope to

estimate the optimal friction coefficient in order to reduce a percentile of the pier response as a function of the safety level required and given an intensity measure related to a seismic ultimate limit state in a specific site.

REFERENCES

[1]   M. C. Constantinou, A. Kartoum, A. M. Reinhorn, P. Bradford , Sliding isolation system for bridges: Experimental study, *Earthquake Spectra* 1992; 8(3): 321-344.

[2]   A. Kartoum, M. C. Constantinou, A. M. Reinhorn, Sliding isolation system for bridges: Analytical study, *J. Struct. Eng.* 1992; 8(3): 345-372.

[3]   P. Tsopelas, M. C. Constantinou, Y. S. Kim, S. Okamoto, Experimental study of FPS system in bridge seismic isolation, *Earthquake Eng. Struct. Dyn.* 1996a; 25(1): 65-78.

[4]   A. Ghobarah, H. M. Ali, Seismic performance of highway bridges, *Eng. Struct.* 1988; 10(3): 157-166

[5]   M. Dicleli, S. Buddaram, Effect of isolator and ground motion characteristics on the performance of seismic-isolated bridges. *Earth. Engin. and Struc. Dyn.* 2006;**35**(2):233-250.

[6]   P. Tsopelas, M. C. Constantinou, S. Okamoto, S. Fujii, D. Ozaki, Experimental study of bridge seismic sliding isolation systems. *Engineering Structures*, Vol. 18, No. 4, pp. 301-310, 1996.

[7]   R.S. Jangid, Seismic Response of Isolated Bridges. *J. Bridge Eng.*, 2004, 9(2): 156-166.

[8]   Jangid, R. S. (2008). Equivalent linear stochastic seismic response of isolated bridges. Journal of Sound and Vibration, 309(3-5), 805-822.

[9]   R. S. Jangid, Stochastic Response of Bridges Seismically Isolated by Friction Pendulum System, *J. Bridge Eng.* 2008; 13(4): (319).

[10] N.P. Tongaonkar, R.S. Jangid, Seismic response of isolated bridges with soil–structure interaction. *Soil Dynamics and Earthquake Engineering* 23 (2003) 287–302.

[11] Olmos, B. A., Jara, J. M., & Roesset, J. M. (2011). Effects of isolation on the seismic response of bridges designed for two different soil types. Bulletin of Earth. Engineering, 9(2), 641-656.

[12] Dehghanpoor, A., Thambiratnam, D., Taciroglu, E., & Chan, T. Soil-pile-superstructure interaction effects in seismically isolated bridges under combined vertical and horizontal strong ground motions. *Soil Dynamics and Earthquake Engineering*, 2019, **126**:105753.

[13] Dehghanpoor, A., Thambiratnam, D., Zhang, W., Chan, T., & Taciroglu, E. An extended probabilistic demand model with optimal intensity measures for seismic performance characterization of isolated bridges under coupled horizontal and vertical motions. *Bulletin of Earthquake Engineering*, 2021, **19**(5), 2291-2323.

[14] L. Su, G. Ahmadi, IG. Tadjbakhsh, Comparative study of base isolation systems. *Journal of Engineering Mechanic* 1989; **115**(9):1976–92.

[15] Yen-Po Wang, Lap-Loi Chung, Wei-Hsin Liao. Seismic response analysis of bridges isolated with friction pendulum bearings. *Earth.Eng.& Str. Dyn.*, 1998; 27, 1069-1093.

[16] VA. Zayas, SS. Low, SA. Mahin, A simple pendulum technique for achieving seismic isolation. *Earthquake Spectra* 1990; **6**(2):317–33.

[17] G. Mosqueda, AS. Whittaker, GL. Fenves, Characterization and modeling of Friction Pendulum bearings subjected to multiple components of excitation. *Journal of Structural Engineering* 2004; **130**(3):433-442.

[18] A. Mokha, MC. Constantinou, AM. Reinhorn, Teflon Bearings in Base Isolation. I: Testing. *Journal of Structural Engineering* 1990; **116**(2):438-454.

[19] MC. Constantinou, A. Mokha, AM. Reinhorn, Teflon Bearings in Base Isolation. II: Modeling. *Journal of Structural Engineering* 1990; **116**(2):455-474.

[20] R. S. Jangid, Computational numerical models for seismic response of structures isolated by sliding systems, *Structural Control and Health Monitoring* 2005; 12:117–137.

[21] MC. Constantinou, AS. Whittaker, Y. Kalpakidis, DM. Fenz, GP. Warn, Performance of Seismic Isolation Hardware Under Service and Seismic Loading. *Technical Report* MCEER-

07-0012, 2007.

[22] JL. Almazàn, JC. De la Llera, Physical model for dynamic analysis of structures with FPS isolators. *Earthquake Engineering and Structural Dynamics* 2003;**32**(8):1157–1184.

[23] N. Bonessio, G. Lomiento and G. Benzoni Damage identification procedure for seismically isolated bridges, *Structural Control and Health Monitoring* 2012; 19:565–578.

[24] L. Landi, G. Grazi, P. Diotallevi, Comparison of different models for friction pendulum isolators in structures subjected to horizontal and vertical ground motions, *Soil Dynamics and Earthquake Engineering* 2016;**81**:75-83.

[25] P. Castaldo, E. Tubaldi, Influence of FPS bearing properties on the seismic performance of base-isolated structures. *Earthquake Engin. and Structural Dynamics* 2015;**44**(15):2817–2836.

[26] P. Castaldo, M. Ripani, Optimal design of friction pendulum system properties for isolated structures considering different soil conditions, *Soil Dynamics and Earthquake Engineering*, 2016, 90:74–87, DOI: 10.1016/j.soildyn.2016.08.025.

[27] E. Tubaldi, L. Ragni, A. Dall'Asta, Probabilistic seismic response assessment of linear systems equipped with nonlinear viscous dampers, *Earthquake Engineering & Structural Dynamics* 2014; DOI: 10.1002/eqe.2461.

[28] Castaldo P., Amendola G., Optimal DCFP bearing properties and seismic performance assessment in nondimensional form for isolated bridges, *Earthquake Engineering and Structural Dynamics*, 2021, **50**(9):2442-2461, https://doi.org/10.1002/eqe.3454.

[29] P. Castaldo, M. Ripani, R. Lo Piore, Influence of soil conditions on the optimal sliding friction coefficient for isolated bridges. *Soil Dynamics and Earth. Engineering*, 2018, 111; 131–148.

[30] Zhang, J., & Huo, Y. (2009). Evaluating effectiveness and optimum design of isolation devices for highway bridges using the fragility function method. *Eng. Structures*, 31(8), 1648-1660.

[31] Kunde, M. C., & Jangid, R. S. (2006). Effects of pier and deck flexibility on the seismic response of isolated bridges. Journal of Bridge Engineering, 11(1), 109-121.

[32] Y. S. Kim, C. B. Yun, Seismic response characteristics of bridges using double concave friction pendulum bearings with tri-linear behavior. *Engin. Struct*. 29, 2007, 3082-3093.

[33] M. Eröz, R. DesRoches. Bridge seismic response as a function of the Friction Pendulum System (FPS) modeling assumptions. *Engineering Structures,* 30 (2008) 3204–3212.

[34] Eröz, M., & DesRoches, R. (2013). The influence of design parameters on the response of bridges seismically isolated with the friction pendulum system (FPS). *Engineering Structures*, 56, 585-599.

[35] P. Castaldo, B. Palazzo, P. Della Vecchia, Life-cycle cost and seismic reliability analysis of 3D systems equipped with FPS for different isolation degrees, *Engineering Structures*, 2016;**125**:349–363, http://dx.doi.org/10.1016/j.engstruct.2016.06.056.

[36] P. Castaldo, B. Palazzo, T. Ferrentino, Seismic reliability-based ductility demand evaluation for inelastic base-isolated structures with friction pendulum devices, *Earthquake Engineering and Structural Dynamics*, 2016; DOI: 10.1002/eqe.2854.

[37] P. Castaldo, G. Alfano, Seismic reliability-based design of hardening and softening structures isolated by double concave sliding devices, *Soil Dynamics and Earth. Eng.*, 129: 105930, 2020.

[38] Panchal, V. R., & Jangid, R. S. Variable friction pendulum system for near-fault ground motions. *Structural Control and Health Monitoring*, 2008. **15**(4):568-584.

[39] Calabrese, A., Quaglini, V., Strano, S., & Terzo, M. Online estimation of the friction coefficient in sliding isolators. *Structural Control and Health Monitoring*, 2020, **27**(3):e2459.

[40] KM. Kelly, *Earthquake-Resistant Design with Rubber*. 2nd ed. Berlin and New York: Springer-Verlag; 1997.

[41] Building Seismic Safety Council. NEHRP Recommended Provisions: Design Examples FEMA 451 - Washington, D.C., August 2006.

[42] MJN. Priestley, F. Seible, GM. Calvi, Seismic design and retrofit of bridges. *Wiley*,1996.

[43] TL. Karavasilis, CY. Seo, N. Makris, Dimensional Response Analysis of Bilinear Systems Subjected to Non-pulse like Earthquake Ground Motions. *J. of Str. Eng.* 2011;**137**(5):600-606.

[44] M. Barbato, E. Tubaldi, A probabilistic performance-based approach for mitigating the seismic pounding risk between adjacent buildings. *Earth. Engin. & Str. Dyn.* 2013;**42**(8):1203-1219.

[45] Kitayama, S., & Constantinou, M. C. Effect of displacement restraint on the collapse performance of seismically isolated buildings. Bulletin of Earthquake Engineering, 2019, **17**(5):2767-2786.

[46] Kitayama, S., & Constantinou, M. C. Probabilistic seismic performance assessment of seismically isolated buildings designed by the procedures of ASCE/SEI 7 and other enhanced criteria. Engine. Struct., 2019, **179**:566-582.

[47] PEER, *Pacific Earthquake Engineering Research Center* http://peer.berkeley.edu/

[48] ITACA, *Italian Accelerometric Archive* http://itaca.mi.ingv.it/ItacaNet/itaca10_links.htm

[49] ISESD, *Internet-Site for European Strong-Motion Data* http://www.isesd.hi.is/ESD_Local/frameset.htm

[50] H. Aslani, E. Miranda, Probability-based seismic response analysis. *Engineering Structures* 2005;**27**(8):1151-1163.

[51] Porter KA. An overview of PEER's performance-based earthquake engineering methodology. Proceedings, *Proceedings of the 9th International Conference on Application of Statistics and Probability in Civil Engineering* (*ICASP9*), San Francisco, California, 2003.

[52] Ryan K, Chopra A. Estimation of Seismic Demands on Isolators Based on Nonlinear Analysis. *Journal of Structural Engineering* 2004;**130**(3):392-402.

[53] Math Works Inc. MATLAB-High Performance Numeric Computation and Visualization Software. User's Guide. Natick: MA, USA; 1997.

[54] T. Karavasilis, C. Seo, Seismic structural and non-structural performance evaluation of highly damped self-centering and conventional systems. *Eng. Structures* 2011,**33**(8):2248-2258.

[55] Ang AHS, Tang WH. Probability Concepts in Engineering-Emphasis on Applications to Civil and Environmental Engineering. John Wiley & Sons, New York, USA; 2007.

[56] Masoud Malekzadeh, Touraj Taghikhany. Multi-Stage Performance of Seismically Isolated Bridge Using Triple Pendulum Bearings. *Advances in Struct. Engineering* Vol. 15 No. 7, 2012.

[57] Evan m. Lapointe. An investigation of the principles and practices of seismic isolation in bridge structures. *Department of Civil and Environmental Engineering*; 2004.

[58] M.C. Kunde, R.S. Jangid, Seismic behavior of isolated bridges: A-state-of-the-art review, *Electronic Journal of Structural Engineering*.2003;Vol. 3.

[59] Michael D. Symans, Steven W. Kelly. Fuzzy logic control of bridge structures using intelligent semi-active seismic isolation systems. *Earthquake Engng. Struct. Dyn*. 28, 37ð60 (1999).

[60] NTC2018. Norme tecniche per le costruzioni. Gazzetta Ufficiale del 20.02.18, DM *Infrastrutture* 17.01.18, Ministero delle Infrastrutture.

[61] L.L. Chung, P.S. Kao, C.Y. Yang, L.Y. Wu, H.M. Chen, Optimal frictional coefficient of structural isolation system. *Journal of Vibration and Control* 2013, Early view. DOI: 10.1177/1077546313487938.

[62] Iemura H, Taghikhany T, Jain S. Optimum design of resilient sliding isolation system for seismic protection of equipments. *Bulletin of Earthquake Engineering* 2007;**5**(1):85-103.

[63] C. Bucher, Probability-based optimization of friction-based seismic isolation devices. *Structural Safety* 2009;**31**(6):500-507.

[64] N. Fallah, G. Zamiri, Multi-objective optimal design of sliding base isolation using genetic algorithm. *Scientia Iranica A*, 2013;**20**(1):87–96.

[65] National cooperative highway research program report 276 – Thermal effects in concrete bridge superstructures, 1985.

[66] Warn Gordon P. and Andrew S. Whittaker, Property Modification Factors for Seismically Isolated Bridges, 2006, 11:3(371), 1084-0702.